UNIVERSITÀ DEGLI STUDI DI TRIESTE

Facoltà di Ingegneria

XX Ciclo del Dottorato di Ricerca in Ingegneria e Scienza dei Materiali

Settore Disciplinare ING-IND/22

Tesi di Dottorato

A HARDWARE FIELD SIMULATOR FOR PHOTOVOLTAIC MATERIALS APPLICATIONS

Dottorando
Ing. Alessandro Massi Pavan

Relatore
Chiar. mo prof. Sergio Roitti

Coordinatore
Chiar. mo prof. Sergio Meriani

ANNO ACCADEMICO 2006-2007

Dedicated to the Earth and to the Sun

Preface

Sustainable development can be defined as living, producing and consuming in a manner that meets the needs of the present without compromising the ability of future generations to meet their own needs. It has become a key guiding principle for policy in the 21^{st} century. Worldwide, politicians, industrialists, environmentalists, economists and theologians affirm that the principle must be applied at international, national and local level.

The concept of sustainable development became widely accepted following the report of the World Commission on Environment and Development (1987). The Commission was set up by the United Nations because the scale and the unevenness of economic development and population growth were, and still are, placing unprecedented pressures on our planet's lands, waters and other natural resources. Some of this pressures are severe enough to threaten the very survival of some regional populations and, in the longer term, to lead to global catastrophes.

Changes in lifestyle, especially regarding production and consumption, will eventually be forced on populations by ecological and economic pressures. Nevertheless, the economic and social pain of such changes can be eased by foresight planning and political will.

World energy use increased more than tenfold over the 20^{st} century. In the 21^{st} century, further increases in world energy consumption can be expected, much for rising industrialization and demand in previously less developed countries.

Fossil fuels are not being newly formed at any significant rate, and thus present stocks are ultimately finite. The dominant fossil fuel type by mass is coal, with oil and gas much less. The reserve lifetime of a resource may be defined as the known accessible amount divided by the rate of present use. By this definition, the lifetime of oil and gas resources is usually only a few decades; whereas lifetime for coal is few centuries. This means that the present patterns of energy consumption and growth are not sustainable in the longer term.

Moreover, economics predict that as the lifetime of a fuel reserve shortens, so the fuel price increases; consequently demand for that fuel reduces and previously more expensive sources and alternatives enter the market.

An other limitation to the fossil fuel use (and indeed nuclear power) are emissions. Increasing concentration of CO_2 in the Atmosphere is such an example. CO_2

emissions from the combustion of fossil fuels have significantly raised the concentration of CO_2 in the Atmosphere. The balance of scientific opinion is that if this continues, it will enhance the greenhouse effect and lead to significant climate change within a century or less.

Therefore for these reasons it is essential to expand renewable energy supplies and to use energy more efficiently because they are much more compatible with sustainable development than are fossil and nuclear fuels, in regard to both resource limitations and environmental impacts. Such conclusions are supported in economics if the full external costs of both obtaining the fuels and paying for the damage from emissions are internalized in the price. Such fundamental analysis may conclude that renewable energy and the efficient use of energy are cheaper for society than the traditional use of fossil and nuclear fuels[1].

Of the same opinion is the European Union: 9 March 2007 was a momentous day for renewable energy in the EU (and arguably in the world). The EU says it will source 20% of its overall energy needs from renewable sources by 2020[2].

[1] Twidell J. and Weir T.: *Renewable energy resources*, Taylor and Francis, 2006, pages 2-4
[2] *20% by 2020: the way forward*, Refocus, Elsevier, March/April 2007

Contents

Introduction

The subject of this work is a power electronic device, hereafter named photovoltaic field simulator, which converts the grid voltage into a current voltage characteristic. This characteristic replicates the behavior of a real photovoltaic field working in arbitrary conditions of irradiance and temperature.

The photovoltaic field simulator will comprise an electronic power converter and a personal computer implemented real time control system.

The photovoltaic field simulator will be used for photovoltaic module parameters design with particular reference to its behavior when inserted in a photovoltaic field operating in shaded conditions. The work will also show why thin-film technologies lead to more problems in a photovoltaic system working under shaded conditions.

The photovoltaic field simulator will also be used for testing power conditioning units[3].

After building, the photovoltaic field simulator will be connected to the experimental photovoltaic plant which will be installed on the roof top of the Materials and Natural Resources Department of Trieste University (hereafter called University of Trieste plant).

The work is divided into five chapters. In the first a brief description of photovoltaic technology is given.

Chapter two is on classic solar cell modelling basics and on the definition of the parameters of photovoltaic technology. This chapter also gives a brief materials and technologies overview.

The third chapter briefly describes photovoltaic grid connected system components. In particular a new model for plotting photovoltaic current voltage and power voltage characteristics is provided. The method is original because only module data sheet parameters are used and experimental measurements are not needed. The model is then developed to describe series and parallel connected modules behavior. Finally, two different photovoltaic plant electrical architectures are described: centralized and string. The chapter gives the fundamental elements

[3] A power conditioning unit converts the direct voltage produced by photovoltaic technology into an alternate sinusoidal 50Hz voltage

for simulator design.

In chapter four the Balance of a photovoltaic System (BOS) is calculated. In particular the importance of the mismatching effect of photovoltaic modules due to shaded conditions is shown.

The last chapter is on simulator description and its applications.

Several of the examples reported refer to the University of Trieste plant whose design was a part of my doctoral work.

This doctoral work is related to one of two activated research lines on photovoltaic technology.

The first regards photovoltaic materials. In particular cadmium telluride thin-film solar cell and quantum dots based intermediate bandgap devices are being developed.

The second research line regards a Laboratory arrangement. The Laboratory will provide instrumentation for photovoltaic cells, modules and systems characterization and check. Tests will be performed both in standard ways and by using ad hoc developed methods (i.e. using the photovoltaic field simulator).

Chapter 1

Photovoltaic technology

Currently, industrial countries generate most of their electricity in large centralized facilities, such as coal power plants, nuclear reactors, hydropower or gas powered plant. These plants have excellent economies of scale, but usually transmit electricity long distances. Coal plants do so to prevent pollution of the cities. Nuclear reactors are thought too unsafe to be in a city. Dam sites are often both unsafe, and intentionally far from cities. The coal and nuclear plants are often considered too far away for their waste heat to be used for heating buildings.

Low pollution is a crucial advantage of combined cycle plants that burn natural gas. The low pollution permits the plants to be near enough to a city to be used for district heating and cooling.

Distributed generation is another approach. It reduces the amount of energy lost in transmitting electricity because the electricity is generated very near where it is used, perhaps even in the same building. This also reduces the size and number of power lines that must be constructed. Typical distributed power sources have low maintenance, low pollution and high efficiencies [1].

Typically distributed generators use renewable sources of energy as solar radiation, hydro-power, wind power, biomass, geothermal, etc.

1.1 State of the art

Approximately $1GW_p$ (for the definition of "W_p" see section 2.1.2) of photovoltaic capacity was installed during 2006 in the countries affiliated to IEA[1]. This is an increase of 36% over the previous year. Most of this increase (82%) was installed in Germany and Japan. Figure 1.1 [2] shows the cumulative growth in photovoltaic capacity since 1992 within the two primary applications for photovoltaic: grid connected and off grid plants (ref. section 3.2). Particularly with the recent levels of

[1] International Energy Agency

growth seen in IEA member countries, the installed capacity reported represents a significant proportion of worldwide photovoltaic capacity.

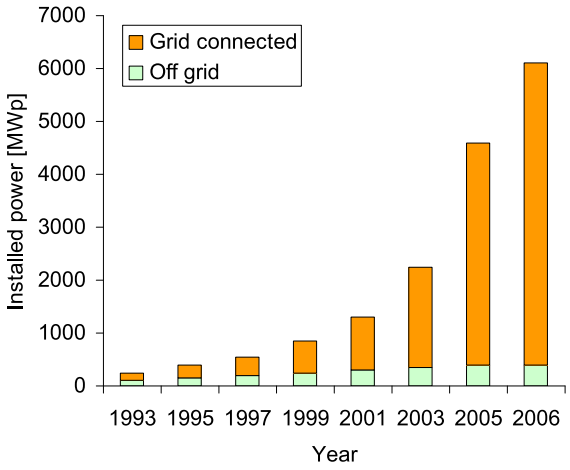

Figure 1.1: Overall installed photovoltaic power in the IEA countries

Figure 1.2 [2] shows the cumulative growth in photovoltaic capacity in Italy. If we compare figures 1.1 and 1.2 we can see that the Italian market started to grow exponentially ten years later than the world market. This was because the feed-in tariff mechanism, which is, and has been, the driver of worldwide photovoltaic growth, was introduced in Italy only in 2005 while in Germany and Japan started already in the 1990s.

1.2 Advantages of photovoltaic technology

The recent interest worldwide in photovoltaic technology has been driven by the following reasons:

1. the fuel source is vast and infinite
2. the technology has near-to-zero operating costs
3. the technology is reliable (plants installed at the end of 1970s are still working today)
4. photovoltaic plants are quick to install

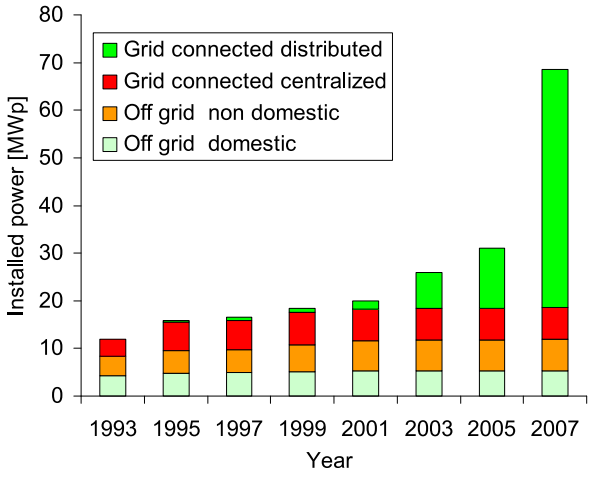

Figure 1.2: Overall installed photovoltaic power in Italy

5. any emission is related to photovoltaic plant operations
6. photovoltaic plants don't have no moving part
7. photovoltaic plants operate at ambient temperature which means no high temperature corrosion or safety issues
8. the technology is modular
9. photovoltaic modules can be integrated into new or existing structures and buildings
10. the technology has an excellent safety record
11. photovoltaic plants are widely accepted by the general public
12. photovoltaic plants can be used at nearly any point of use
13. photovoltaic plants daily output peak may match local demand

1.3 Italian subsidies

As reported in section 1.1, the world wide photovoltaic technology exponential growth has been driven the feed-in tariff mechanism.

At last we are at a turning point. After too many years of photovoltaic financing through rebate programs, promoted by Regions and by the Ministry of Environment, the Italian feed-in tariff was signed on July 2005 by the Italian Ministry of Industry [3]. The result has been the enormous increase in installed power seen during year 2007 and shown in figure 1.2.

The Italian feed-in tariff mechanism is split into two different categories of photovoltaic plants: plants for which it is allowed to use the net meetering mechanism and plants for which is not. Figure 1.3 shows the feed-in tariff mechanism when the net meetering is allowed. In this case the costumer has the possibility to use the electrical grid as an ideal battery: when the production exceeds the electrical loads consumption the excess energy is delivered to the grid while when the sun is not shining the energy is provided by the grid. A first electricity meter C_1 measures the energy produced by the photovoltaic plant while a second electricity meter C_2 measures the difference between the energy delivered and the energy absorbed from the grid so that the costumer pays only for the kWhs exceeding the photovoltaic production. If the costumer consumes all the annual energy produced, the year cash flow is:

$$CF = C_1 \times (\alpha + \beta) \tag{1.1}$$

where C_1 is the photovoltaic plant year production, α is a refund which the Italian government gives to the photovoltaic plant owner for any produced kWh and β is the kWh cost for the costumer (an average value is 0.15€). The value of α [€/kWh] depends on the photovoltaic plant size and on its architecture integration level as described in table 1.1 [4]. The refund α is given to the photovoltaic plant owner for 20 years of plant operations.

Rated power [kW_p]	Not integrated	Partial integrated	Integrated
1-3	0.40	0.44	0.49
3-20	0.38	0.42	0.46
$>$20	0.36	0.40	0.44

Table 1.1: Italian incentives for grid connected plants

Figure 1.4 shows the feed-in tariff mechanism when the net meetering is not allowed. In this case there are two connections with the utility grid: one connection powers the electrical loads and the second is dedicated to the photovoltaic plant. In this case the annual cash flow is:

$$CF = C_2 \times (\alpha + \gamma) \tag{1.2}$$

where C_2 is the photovoltaic plant year production and γ is the sale tariff which depends on the market (an average value is 0.08€).

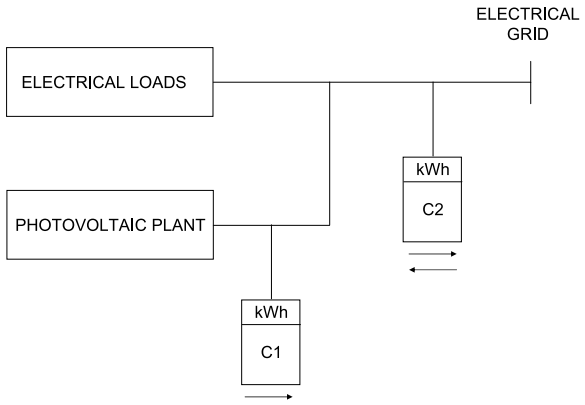

Figure 1.3: Feed-in tariff mechanism: net meetering allowed

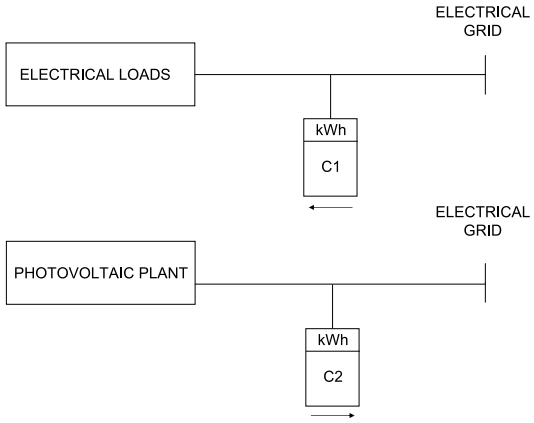

Figure 1.4: Feed-in tariff mechanism: net meetering not allowed

Tables 1.2 and 1.3 [5] show the situation in the Italian photovoltaic market on March 31st 2006. Table 1.2 shows that the most popular size plants (99% of them) are smaller than 50kW_p while table 1.3 indicates that most of the cumulative power is concentrated in medium size plants (20-50kW_p).

Rated power [kW_p]	Number of plants	[%]
1-20	7176	58
20-50	5105	41
>50	152	1
Total	12433	100

Table 1.2: Number of required photovoltaic plant installations

Rated power [kW_p]	Cumulative power [MW_p]	[%]
1-20	51.4	13
20-50	237.2	61
>50	99.1	26
Total	387.7	100

Table 1.3: Required photovoltaic plant installations: cumulative power

1.4 Economic analysis

The purchase of a photovoltaic system represents an expenditure of capital resources at a given time with the expectation of benefits in the form of electric energy delivered over the technical life of the system. Thus the operation of a photovoltaic system involves a stream of cash flow over some years, and economic assessment requires a proper measurement of both outflows, as the purchase cost and maintenance costs, and inflows, as the value of electricity produced and/or the value of savings (cheaper bill) due to the local consumption of the energy produced by the photovoltaic plant [6].

As an example consider a $20kW_p$ integrated photovoltaic plant built in Rome. We want to calculate the investment payback period and its economic productivity under feed-in tariff when net meetering is allowed.

It is possible to calculate the above values by applying a cash flow analysis to the photovoltaic system:

$$NPV = -I_0 + CF \times \sum_{i=1}^{n} \frac{1}{(1+d)^i} - \sum_{i=1}^{n} MC_i \tag{1.3}$$

where NPV is the investment net present value, I_0 is the initial investment, CF is the annual cash flow, d is the discount factor, MC is the annual maintenance cost and n is the investment lifetime. The investment lifetime for feed-in tariff incentivate photovoltaic plants is 20 years. It is important to note that the plant lifetime will be longer than 20 years: typical lifetime for this type of plants is more than 30 years. If a photovoltaic plant averaged cost of 6.500,00€/kW_p is assumed,

the example initial investment is I_0 = 130.000,00 €. For equation 1.1, the annual cash flow CF [€] is given by:

$$CF = 20 \times 1.450 \times (0,46 + 0,15) = 17.690,00 \tag{1.4}$$

where 1.450 is the productivity (ref. section 4.1.1) of a $1kW_p$ photovoltaic plant built in Rome (latitude 41.9°) having a South exposition and an inclination of the photovoltaic modules of 30°; the assumed reflectivity is 22% (concrete blocks) while a 80% of Balance Of System has been assumed (ref. section 4.1). The discount factor is:

$$d = r - f - t = 5 - 2 - 2 = 1\% \tag{1.5}$$

where r is the interest rate, f the inflation rate and t the drift rate of the energy cost compared to inflation. The annual maintenance cost has been calculated as the 0.3% of the photovoltaic plant cost.

From figure 1.5, which shows the cash analysis result, there is a payback period of eight years and three mounts.

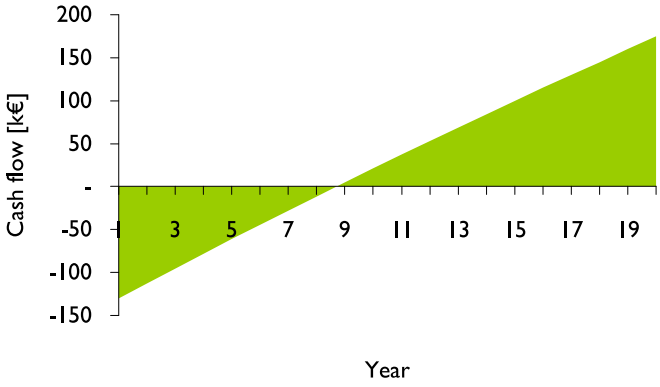

Figure 1.5: Cash flow analysis: photovoltaic plant built in Rome

The investment productivity is given by:

$$IP = \frac{NPV + I_0}{n \times I_0} = 12\% \tag{1.6}$$

The cash analysis shown above proves that the introduction of the feed-in tariff mechanism in Italy makes photovoltaic plant investments not only possible but

also a really good long term investment. It is in fact not easy (well nigh impossible) to find a long term investment which is as certain as this and has such a high productivity. For this reason it seems possible to have even a bigger rate of growth compared to Germany in forthcoming years for solar technology in Italy. Consider in fact a plant built in Freiburg (which is called the sun city because of its many photovoltaic plants and industries): at this latitude (48°), the plant productivity is 1000kWh/year [7] corresponding to the cash flow analysis shown in figure 1.6. The results are: a time back period of 11.5 years and a investment productivity of 8.3%. Even if these figures are significantly less interesting for investors, the German photovoltaic market is today driving the worldwide market.

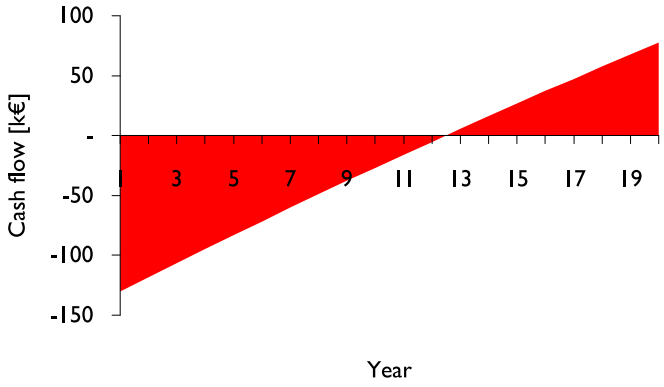

Figure 1.6: Cash flow analysis: photovoltaic plant built in Freiburg

Bibliography

[1] http://en.wikipedia.org/wiki/Distributed_generation#Distributed_energy_resources

[2] *Trends in photovoltaic applications. Survey report of selected IEA countries between 1992 and 2006*, International Energy Agency, 2006

[3] *Dolce vita for pv in Italy? New feed-in tariff introduced for the Italian PV market*, Refocus, Elsevier, September/October 2005

[4] Italian law: *Decreto Legislativo 19 febbraio 2007*, N. 45

[5] http://www.grtn.it/

[6] Luque A. and Hegedus S.: *Handbook of photovoltaic science and engineering*, Jhon Wiley and Sons Inc., 2006, pages 971, 972 and 973

[7] http://re.jrc.ec.europa.eu/pvgis/

Chapter 2

Fundamentals and technologies

Introduction

Photovoltaic is the technology that generates Direct Current (DC) from semiconductors when they are illuminated by photons. As long as light is shining on the solar cell, while it is connected to a load, it generates electrical power. When the light stops, the electricity stops.

Solar cells are made of semiconductors materials. In a semiconductor the electrons occupying the valence band are weakly bonded. When an energy exceeding the band gap of the materials is applied to a valance electron, the bonds are broken and the electron is free to move in the conduction band. The energy can be supplied to the electron by photons, particles of light.

Figure 2.1 [1] shows the outline of a solar cell. When the cell is exposed to sunlight, photons hit valence electrons, breaking the bonds and pumping them to the conduction band. An external contact that collects the conduction band electrons drives these electrons to the external circuit. The electrons lose their energy by doing work in the external circuit and they are restored to the solar cell via a second contact, which returns them to the valence band with the same energy that they started with.

In reality a solar cell is simply a diode that has bees carefully designed and constructed to efficiently absorb and convert light energy from the sun into electrical energy [1]. A simple conventional solar cell is shown in the figure 2.2 [1]. Solar light falls from above to the front of the solar cell. A metallic grid forms one of the electrical contacts of the diode and allows the light to fall on the material between the grid lines and thus be absorbed and converted into electrical energy. An antireflective layer between the grid lines increases the amount of light transmitted to the semiconductor.

The diode is made when an n-type and an p-type semiconductor are put together to form a metallurgic junction. The other electrical contact of the diode is formed

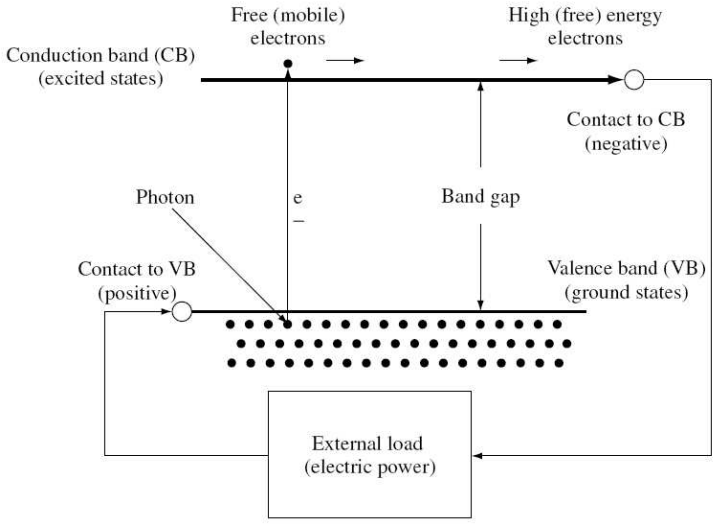

Figure 2.1: Outline of a solar cell

by a metallic layer on the back of the solar cell.

When photons carried by sunlight have a sufficient energy, greater than the material band gap, they can create an electron-hole couple. The energy carried by the photons is expressed by:

$$E_\lambda = \frac{hc}{\lambda} \tag{2.1}$$

where λ is the wavelength, h is Plank's constant and c the speed of light.

Thus, the spectral nature of sunlight is a key in the design of solar cells.

2.1 Fundamentals of a solar cell

The basic *current voltage (I-V) characteristic* of a solar cell can be found by solving the minority-carrier diffusion equation with appropriate boundary conditions [1]. The result is:

$$I = I_{sc} - I_{o1}(e^{qV/kT} - 1) - I_{o2}(e^{qV/2kT} - 1) \tag{2.2}$$

where I_{sc} is the short circuit current, I_{o1} is the dark saturation current due to the recombination in the quasi-neutral regions, I_{o2} is the dark saturation current due to the recombination in the space-charge regions, q is the electron charge, k is Boltzmann's constant and T is the cell temperature.

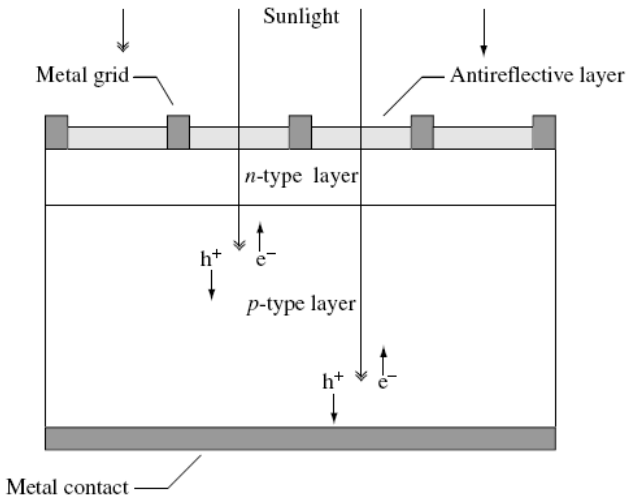

Figure 2.2: Conventional solar cell

The short circuit current and the dark saturation currents depend on the solar cell structure, materials properties and on operating conditions.

Equation 2.2 describes the simple solar cell circuit shown in figure 2.3.

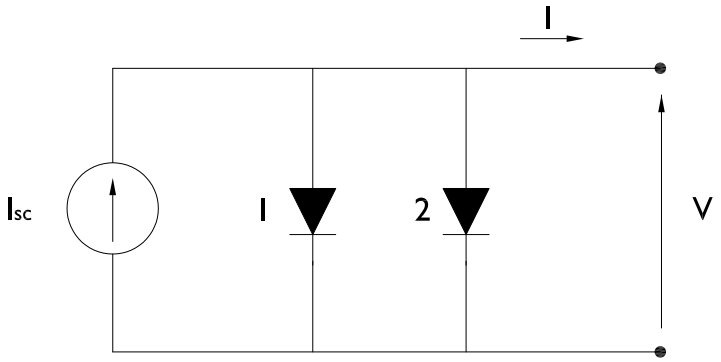

Figure 2.3: Simple solar cell circuit model

The I-V characteristic of this simple model is shown in figure 2.4 where I_{o2} has been neglected (a reasonable assumption for a good silicon solar cell).

Picture 2.4 shows three important figures of a solar cell: the solar cell *short circuit current* I_{sc}, the solar cell *open circuit voltage* V_{oc} and the solar cell *maximum power operating point* P_{mp}. Of particular interest is P_{mp}: at this operating point the power produced is the maximum deliverable to the load. This point is charac-

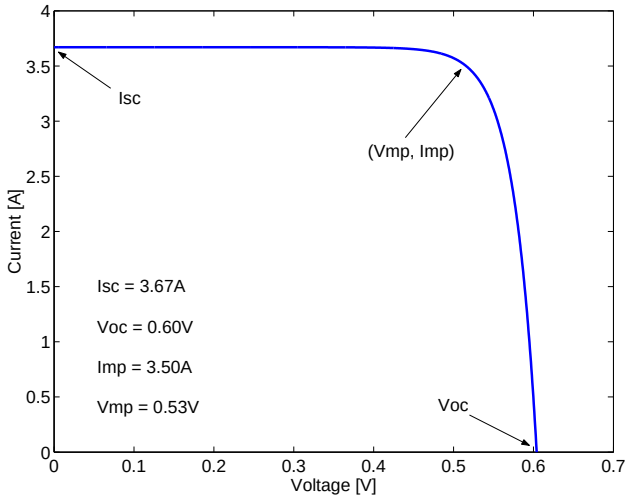

Figure 2.4: Simple solar cell I-V characteristic

terized by the *maximum power point voltage* $V = V_{mp}$ and by the *maximum power point current* $I = I_{mp}$. As shown in figure 2.4, the maximum power point defines a rectangle whose area is the largest rectangle for any point on the I-V curve.

Another important figure is the solar cell *fill factor* (always less than 1), the measure of the squareness of the current voltage characteristic, which is defined as:

$$FF = \frac{V_{mp} \times I_{mp}}{V_{oc} \times I_{sc}} \tag{2.3}$$

Finally, it is fundamental to consider the solar cell *efficiency* which is defined by:

$$\eta = \frac{P_{mp}}{P_{in}} \tag{2.4}$$

By multiplying equation 2.2 by the voltage V a *power voltage characteristic (P-V)* can be obtained. A solar cell P-V characteristic is shown in figure 2.5.

In figure 2.5 the maximum power operating point P_{mp} and the correspondent maximum power point voltage V_{mp} are shown.

2.1.1 Parasitic resistance effect

Equation 2.2 neglects the parasitic series and shunt resistances typically associated with real solar cells. Equation 2.5 [1] takes into account this two resistances:

$$I = \overline{I_{sc}} - I_{o1}(e^{q(V+IR_s)/kT} - 1) - I_{o2}(e^{q(V+IR_s)/2kT} - 1) - \frac{V + IR_s}{R_{sh}} \tag{2.5}$$

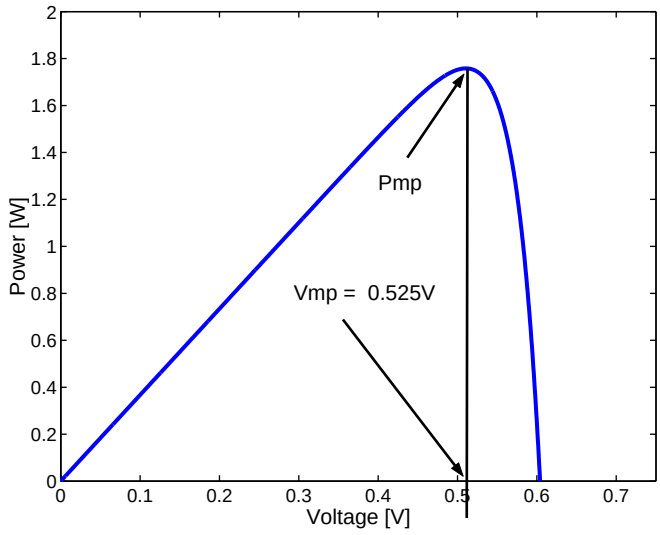

Figure 2.5: Solar cell P-V characteristic

where $\overline{I_{sc}}$ is the short circuit current when there is no parasitic resistance, R_s is the series resistance and R_{sh} is the shunt resistance. From equation 2.5, the series resistance reduces the solar cell short circuit current while the shunt resistance reduces the open circuit voltage.

Equation 2.5 describes the circuit shown in figure 2.6. Figures 2.7 and 2.8 [1] show the influence of the parasitic resistances.

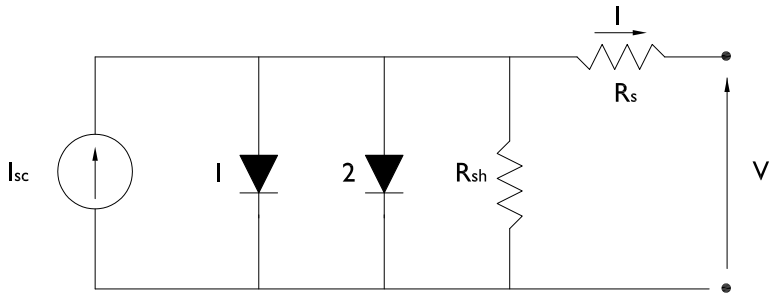

Figure 2.6: Solar cell circuit including parasitic resistances

It is convenient re-write equation 2.5 as:

$$I = \overline{I_{sc}} - I_o(e^{q(V+IR_s)/AkT} - 1) - \frac{V + IR_s}{R_{sh}} \tag{2.6}$$

where A is the diode ideality factor: typically values are between 1 and 2.

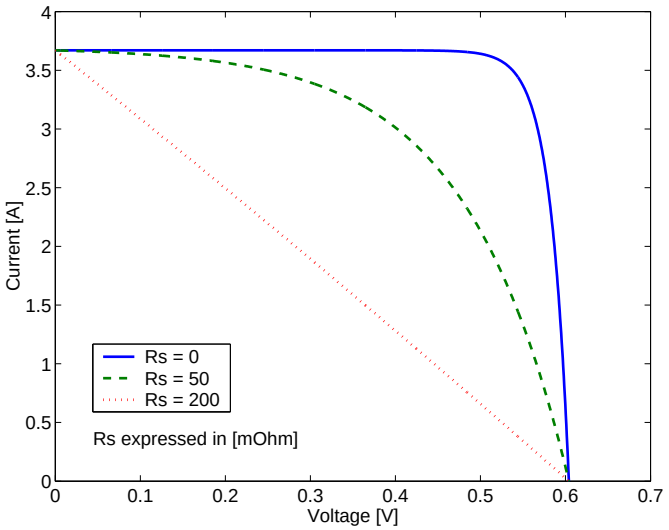

Figure 2.7: Effect of series resistance

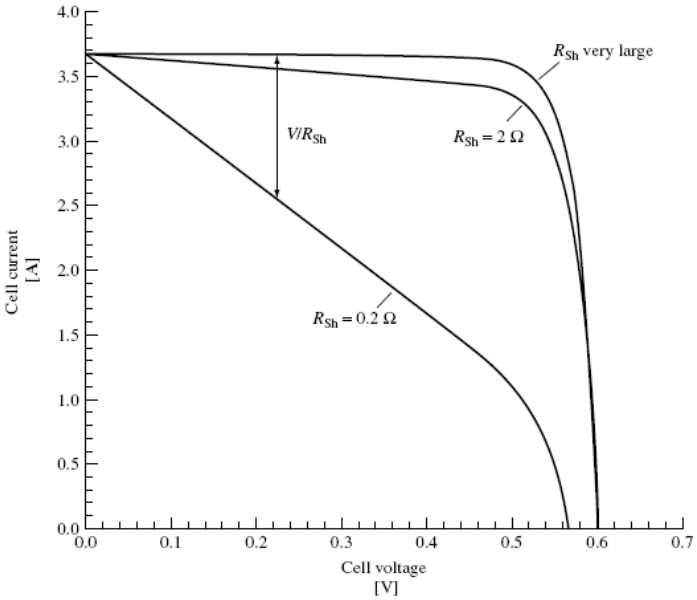

Figure 2.8: Effect of shunt resistance

2.1.2 Standard Test Conditions

Since the electrical characteristics of a solar cell depend on the working climate conditions (solar cell temperature and irradiance), it is customary to estimate these

under the so-called *Standard Test Conditions* (STC):

1. irradiance: $1000 W/m^2$
2. solar spectrum: AM 1.5
3. cell temperature: 25°C

The values of the solar cell short circuit current, the open circuit voltage, the maximum power point current and the maximum power point voltage reported in a solar cell data-sheet are always referred to STC.

The power produced by a photovoltaic cell under STC is known as solar cell *peak power* $[W_p]$.

2.1.3 Dependance on solar cell temperature

The principal effect of temperature on a solar cell comes from the temperature dependance of the open circuit voltage which can be described by:

$$V_{oc}(T_c, G) = V_{oc} + w(T_c - 25) \tag{2.7}$$

where T_c is the operating cell temperature, G is the irradiance, V_{oc} is the open circuit voltage at STC, and $w = dV_{oc}/dT$ is the temperature coefficient. If an accurate measured value of w is not known, the following expression can be used:

$$w = \frac{V_{oc} - E_{g0} - \gamma k_B T_c}{T_c} \tag{2.8}$$

where E_{g0} [eV] is the material energy gap at 0K, $k_B T_c$ [eV] is the thermal energy and γ is a constant (set to three for silicon) [2].

The cell temperature T_c can be calculated as:

$$T_c = T_a + \frac{NOCT - 25}{1000} G \tag{2.9}$$

where T_a [°] is the ambient temperature, *NOCT* [°] is the *Nominal Operating Cell Temperature* and G $[W/m^2]$ is the irradiance. If *NOCT* is not known, a reasonable value is 48°C (silicon solar cell) [2].

Figure 2.9 shows the solar cell I-V characteristic dependance on temperature; irradiance has been set to $1000 W/m^2$.

As shown in figure 2.9, an increase in solar cell temperature is met with a decrease in solar cell open circuit voltage. On the other hand, a change in solar cell temperature does not correspond to a appreciable change in solar cell short circuit current.

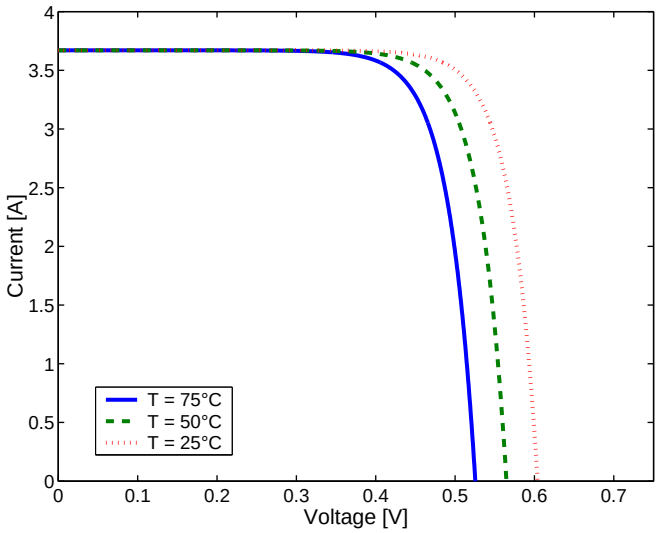

Figure 2.9: I-V solar cell characteristic: dependance on cell temperature

2.1.4 Dependance on irradiance

Figure 2.10 shows the solar cell I-V characteristic dependance on irradiance; cell temperature has been set to 25°C.

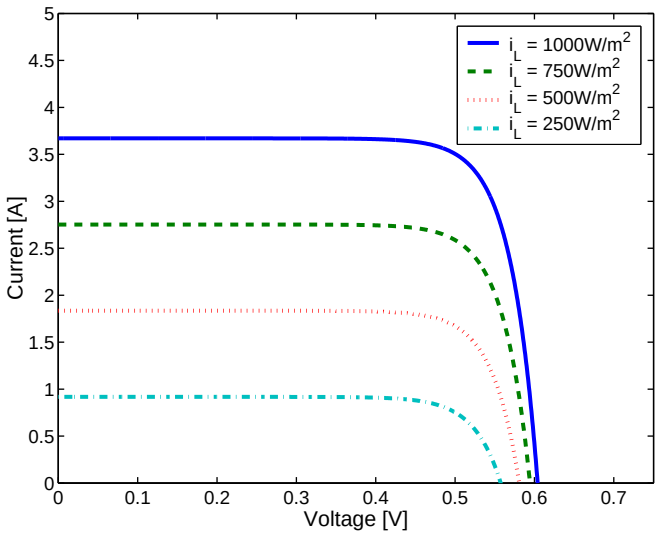

Figure 2.10: I-V solar cell characteristic: dependance on irradiance

As shown in figure 2.10, a decrease in irradiance is met with both a decrease in solar cell open circuit voltage and short circuit current.

2.2 A technology overview

2.2.1 Introduction

Figure 2.11 (year 2003, dollars) [3] shows the efficiency-cost trade-off for the three generations of solar cell technology: wafers, thin films and advanced thin-films.

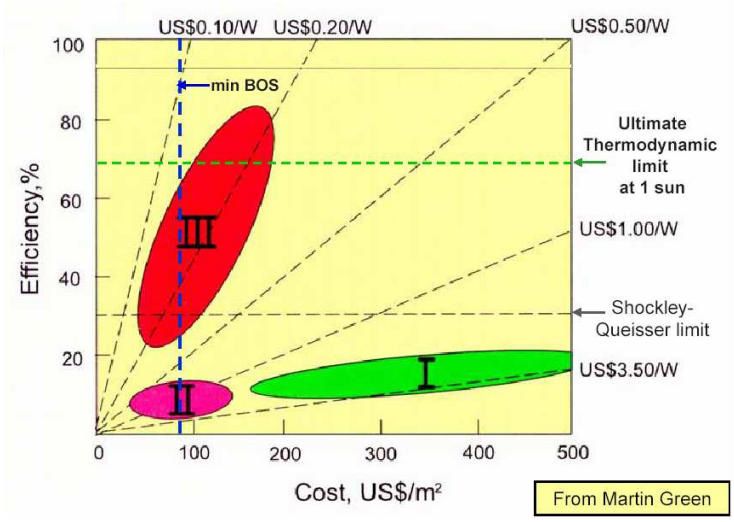

Figure 2.11: Efficiency-cost trade-off for the three generation of solar cell technology

The first solar cell technology is based on silicon either single or multi crystalline wafers (hereafter c-Si). This technology started in the 1950s and was driven forward by the progress in manufacturing of integrated circuit chips and by silicon band gap, 1.1eV, which is almost optimum for a solar cell (ref. figure 2.12 [4]). The principle characteristic for this type of solar cells is a huge use of active material (as shown in figure 2.14 the thickness of a c-Si solar cell is hundreds of μm) which means there is little potential for cost reduction.

The second technology regards thin-film based solar cells which have been produced from the early 1980s. The principal characteristic of this generation is the substantial reduction in materials cost (in this case the solar cell thickness is few μm as indicated in figure 2.17). On the other hand, the efficiency of these solar cells is lower than the first generation. This technology includes mainly amorphous silicon (a-Si), copper indium diselenide $CuInSe_2$(CIS), copper indium gallium diselenide $Cu(InGa)Se_2$ (CIGS), copper indium gallium sulphur diselenide $CuInGaSSe$

(CIGSS), and cadmium telluride *CdTe*.

The third generation regards devices which are significantly more efficient than the first generation. Moreover, the cost of this technology is again lower than the first one. The technology mainly includes multi-junction cells, intermediate band cells, organic cells, etc.

In short, the first generation has medium values of efficiency and high production costs with few possibilities of reduction, the second generation offers lower costs but poor values of efficiency while the third one is expected to be the leading technology with great improvements in efficiency and in manufacturing costs.

The values of solar cell efficiency, open circuit voltages and short circuit currents are listed in table 2.1 [5]. The multi-junction $GaInP/GaAs/Ge$ space solar cell is the best with an efficiency of 32%. This is followed by the thin-film $GaIAs/CIS$ with a 25.8% and the Si (crystalline) solar cell rated 24.7%.

Classification	η [%]	V_{oc} [V]	I_{sc} $[mA/cm^2]$	FF [%]
Silicon				
Si (crystalline)	24.7 ± 0.5	0.706	42.2	82.8
Si (multicrystalline)	20.3 ± 0.5	0.664	37.7	80.9
Si (amorphous)	9.5 ± 0.3	0.859	17.5	63.0
III-V Cells				
GaAs (crystalline)	25.1 ± 0.8	1.022	28.2	87.1
GaAs (thin-film)	24.5 ± 0.5	1.029	28.8	82.5
GaAs (multicrystalline)	18.2 ± 0.5	0.994	23.0	79.7
Thin-film Chalcogenide				
CIGS	18.4 ± 0.5	0.669	35.7	77.0
CdTe	16.5 ± 0.5	0.845	25.9	75.5
Photochemical				
Dye sensitised	10.4 ± 0.3	0.729	21.8	65.2
Organic				
Organic Polymer	3.0 ± 0.1	0.538	9.68	52.4
Multi-junction Devices				
GaInP/GaAs/Ge	32.0 ± 1.5	2.622	14.37	85.0
GaInP/GaAs	30.3	2.488	14.22	85.6
GaIAs/CIS (thin-film)	25.8 ± 1.3			

Table 2.1: Cells STC electrical data

Table 2.2 [5] reports photovoltaic module efficienciy, open circuit voltages and short circuit currents.

Finally table 2.3 [6] gives the distribution of photovoltaic cell production by technology in 2006: multi-crystalline Si (mc-Si), single-crystal Si (sc-Si), amor-

Classification	η [%]	V_{oc} [V]	I_{sc} [A]	FF [%]
Si (crystalline)	22.7 ± 0.6	5.6	3.93	80.3
Si (multicrystalline)	15.3 ± 0.4	14.6	1.36	78.6
Si (thin-film)	8.2 ± 0.2	25.0	0.318	68.0
CIGSS	13.4 ± 0.7	31.2	2.16	68.9
CdTe	10.7 ± 0.5	26.21	3.205	62.3

Table 2.2: Modules STC electrical data

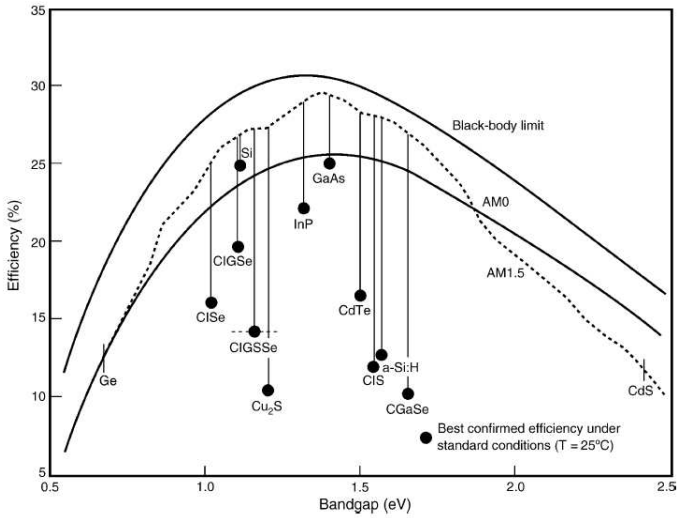

Figure 2.12: Efficiency versus band gap for different materials

phous Si (a-Si), ribbon Si, CdTe and copper indium diselenide (CIS). The solar cells market is covered for the 98.2% by Si technology.

Figure 2.13 [7] shows that the production of photovoltaic modules has been every year less than the production capacity. This phenomena, which is due to the problem of electronic grade feedstock supplying, added to the Si monopoly clearly indicates the need to move away from the first generation of solar cells.

2.2.2 First generation

Of the more than $1GW_p$ of PV commercial shipments in 2004, a dominant 94% were single-crystal, multicrystalline, ribbon, and sheet silicon [8]. In fact, the market would have absorbed even more except that the supplies were limited due to insufficient manufacturing capacities and supplies [9-10].

As mentioned in the introduction, c-Si technology is expensive because of the

Technology	Production [%]
mc-Si	52.3
sc-Si	38.3
a-Si	4.7
ribbon Si	2.9
CdTe	1.6
CIS	0.2

Table 2.3: Technology distribution of photovoltaic cell production

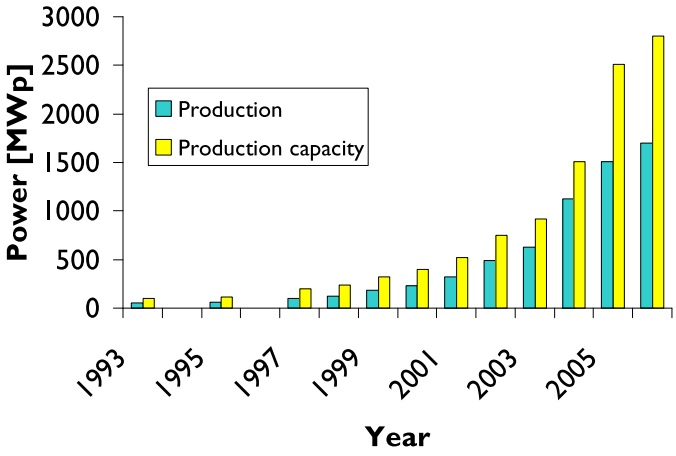

Figure 2.13: Technology photovoltaic module production between 1993 and 2006

large amount of material needed to built the solar cell. Furthemore, crystalline solar cell efficiency, today at 24.7%, corresponds to the 85% of its reported theoretical limit. This means there is little left in c-Si research.

On the other hand c-Si is today the most important solar technology for three fundamental reasons:

1. only c-Si modules can satisfy many rooftop applications because of their high efficiency value
2. the technology is stable
3. the technology is durable

The terrestrial commercial ”20% efficiency club” [4] is represented by the three

solar cells shown in figures 2.14, 2.15 and 2.16 [4]. These are three different approaches that are leading toward the 20% c-Si module today.

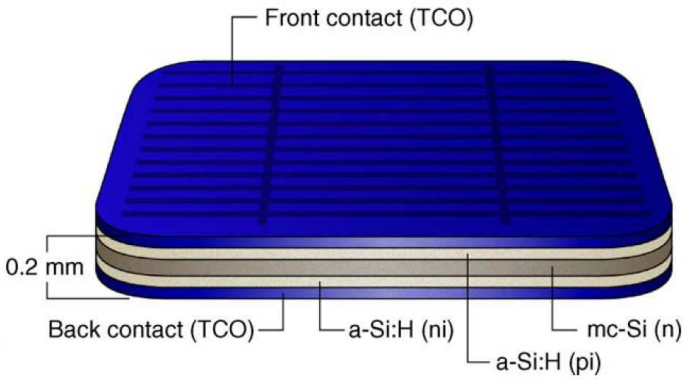

Figure 2.14: Sanyo HIT crystalline Si solar cell

The solar modules used for the University of Trieste plant (ref. section 3.1.1) are made of Sanyo HIT solar cells shown in figure 2.14. In this case a n-type single-crystal wafer surrounded by ultra-thin a-Si:H films in a bifacial structure is employed. The a-Si:H is an hydrogenated amorphous silicon where hydrogen plays an important role in determining optoelectronic properties; in particular removes defects and their states in the gap and also widens the gap.

Both front and back contacts are realized by using a *Transparent Conductive Oxide* (TCO). Some examples of TCO materials are tantalum oxide Ta_2O_5, zinc oxide ZnO, indium oxide In_2O_3 (ITO), cadmium stannate Cd_2SnO_4 (CTO), zinc stannate Zn_2SnO_4 (ZTO), etc. All these materials must have high optical transparency in the wavelength range 400 to 1000 nm, a good conductivity and the ability to form a good contact. This cell efficiency is 20.1% while module efficiency exceeds 16%.

The BP Solar Saturn solar cell (shown in figure 2.15) peculiarity is the minimized front contact area by burying the contacts in laser-produced grooves that lower the resistance through enhanced sidewall areas. The cell efficiency is in this case 20.5%.

Finally the Sun Power A-300 solar cell (shown in figure 2.16) is engineered to contact from the rear side with no light obscuration on the front surface. The measured efficiency for this solar cell is 21.5%.

Tables 2.4 and 2.5 [4] show the cost and the energy breakdown structures for c-Si technology. Module finishing includes encapsulation materials, glass, frame, contacting/wiring, junction boxes, etc. A major consideration with the cost of producing the c-Si cell is associated with producing the high-perfection wafer. For this

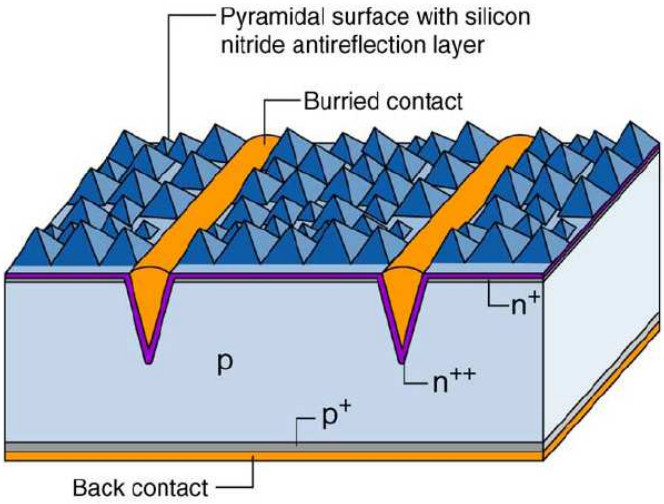

Figure 2.15: BP Solar Saturn crystalline Si solar cell

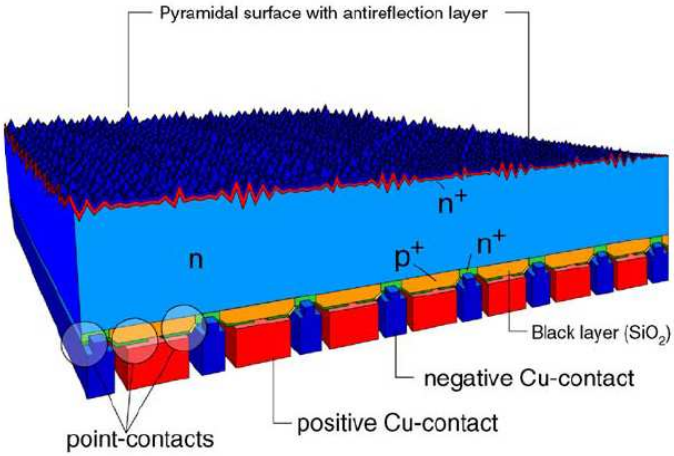

Figure 2.16: Sun Power A-300 crystalline Si solar cell

reason casting of lower-purity feedstock materials has become the manufacturing standard practice: in this case we refer to multicrystalline silicon (m-Si). This has meant less energy costs but on the other hand the efficiency devices has decreased (typical values for m-Si photovoltaic modules are 11-13%).

Activity	Energy required [%]
Silicon	59
Cell	22
Module finishing	18

Table 2.4: Energy breakdown structures for c-Si technology

Activity	Cost [%]
Silicon	50
Cell	20
Module finishing	30

Table 2.5: Cost breakdown structures for c-Si technology

2.2.3 Second generation

Thin-film silicon solar cells

About 30 years ago, the first thin-film silicon solar cell based on hydrogenated amorphous silicon (a-Si:H) was reported [29]. Thin-film silicon solar cells have a smaller thickness compared to crystalline solar cells. This is a plus point because of competition with the microelectronic market which has caused a dangerous silicon shortage for the photovoltaic industry in the past and may cause greater problems in the near future. Furthmore, the smaller thickness of this technology may potentially bring about a reduction in the cost of solar cells and modules, lighter devices, the opportunity for lower energy consumption during cell fabrication, and, finally, make it easy to obtain flexible devices.

A further advantage of thin-film silicon solar cells, as no other thin-film material, is that they are very effective in tandem and triple-junction solar cells (ref. section 2.2.4) [24].

The larger band gap than crystalline silicon (1.7-1.9eV versus 1.1eV) means to higher open circuit voltage and cell fill factor.

On the other hand, the high band gap associated with this technology means lower photocurrent because of a limited absorption of the solar spectrum. Moreover, another important point to notice is that the light induced degradation of these devices leads to a reduction in solar cells efficiency after a short period of operation.

The advantages discussed above make thin-film silicon solar cells very attractive for the future. Production in practice of solar cells with the above advantages poses many challenges in both design and device fabrication [1].

As an example, a commercial a-Si:H solar cell is shown in figure 2.17 [4]. The cell is based on the crystalline silicon on glass (CSG) technology [27-28]. The

cross-section of the CSG solar cell shows that the substrate is textured glass with a silicon nitride deposited surface layer. Over this surface three layers of different doped a-Si:H have been deposited. A low-cost "optically non-absorbing resin, electrically insulating" is applied in two stages: the first producing the negative crater contact regions, the second making the positive dimple contacts to the p-layer. Finally, aluminum is deposited over the entire surface. Prototype modules in the 8% efficiency regime have been reached, and the expectation is to reach 10% making this a viable commercial product [4].

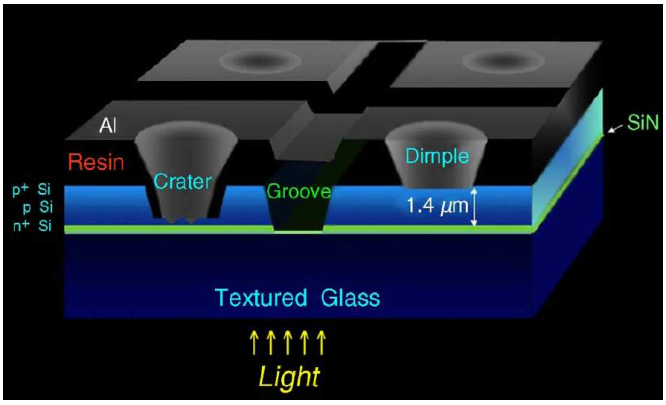

Figure 2.17: Cross section of a thin-film Si solar cell crystalline silicon

Cadmium telluride

Since the 1960s, *CdTe* has been a candidate photovoltaic material first for space, and now the leading terrestrial product [11]. This technology have been fabricated by a variety of of potentially scalable and low-cost processes, including physical deposition, spraying, screen printing/sintering and electrodeposition [12]. Cadmium telluride and copper indium diselenide alloy thin-film photovoltaic modules are entering the renewable energy marketplace in increasing volume, with more than a dozen companies worldwide engaged in startup and manufacturing [13].

With reference to figure 2.18 [4], where a representative cross-section of the device is shown with a corresponding SEM micrograph, the cadmium telluride solar cell is fabricated in a superstrate configuration, rather than the more common substrate configuration. This means that the glass is used as a substrate for the deposition of all layers is the side exposed to the sun. The junction is made of the couple cadmium sulfide *CdS*, which is n-doped, and the cadmium telluride *CdTe*, which is p-doped. The photons coming from the sun go through the glass, through the couple Cd_2SnO_4/Zn_2SnO_4, through the thin layer of cadmium sulfide, and are then absorbed in the cadmium telluride layer. This layer can be thin (from 3 to

8 microns), because cadmium telluride has a direct band gap and therefore a high absorption coefficient. This is the great advantage of using this technology instead of the costumary silicon technology (silicon has poor absorption so that usually more than 200 microns have to be used, with great cost and supply issues). Moreover, cadmium telluride has a really good band gap (1.5 eV). Maximum theoretical efficiencies with cadmium telluride based devices is around 30%.

The couple Cd_2SnO_4/Zn_2SnO_4 makes the front contact layer while a metal, which can be copper or gold, makes the back contact.

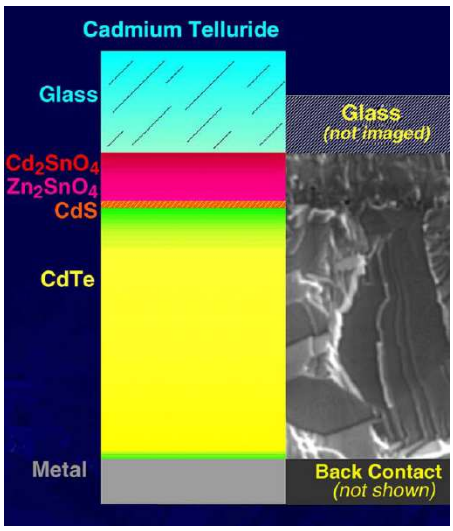

Figure 2.18: Cross sectional representation of a CdTe solar cell

Although there are concerns, perceptions and misconceptions about the environmental, safety and health effects of the *Cd* in this device, extensive studies indicate that all safety issues can be handled with modest investment in cost, recycling of the materials and modules and tracking of deployed product [14].

CIS, CIGS and CIGSS

Since the early 1970s, $Cu(InGa)Se_2$ based solar cells have often been touted as being among the most promising of solar cell technologies for cost-effective power generation. This is partly due to the advantages of thin films for low-cost, high-rate semiconductor deposition over large areas using layers only a few microns thick and for fabrication of monolithically interconnected modules [1].

Perhaps more importantly, very high efficiencies for thin-film technologies have been demonstrated with $Cu(InGa)Se_2$ at both the cell and the module levels. Finally differently from thin-film silicon solar cells, $Cu(InGa)Se_2$ solar cells and modules have shown excellent long-term stability in outdoor testing [15].

Figure 2.19 [4] shows a CIGS solar cell cross sectional representation with a SEM micrograph of the various layers.

In this case the back contact is obtained on a soda-lime glass substrate via sputtering a molybdenum thin-film while the front contact is made of two thin-film layers of aluminum and nichel. The absorber is represented by the copper indium gallium diselenide $Cu(InGa)Se_2$ thin-film which is deposited (there are several methods including chemical deposition, electro-chemical techniques, etc.) on the top on the *Mo* back electrode. The heterojunction is finally completed by a chemical bath deposition of a cadmium sulfide CdS layer.

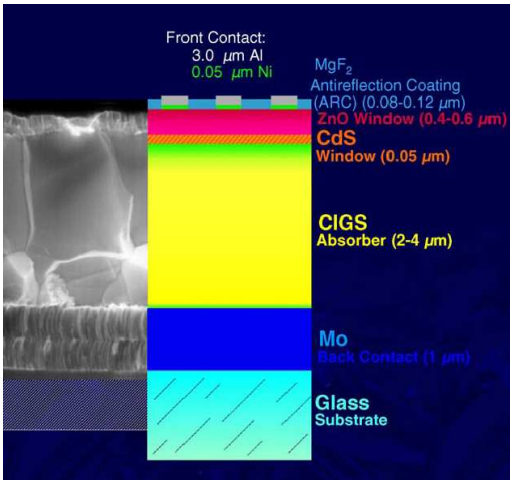

Figure 2.19: Cross sectional representation of a CIGS solar cell

Looking toward the materials demands for multi-megawatts of this technology, current research has focused on reducing the thickness of the absorber from the $2.5\mu m$ regime to less than $1\mu m$ [34]. One objective is to reduce the amount of *In* used - a material that has issues with availability, competition from the large and growing flat-panel display industry, and recent price rises [4].

Dye-sensitized solar cells

The difference between this type of device and all the others reviewed in this work is that in this case the materials used to make the photoelectric phenomena is not a solid.

As shown in figure 2.20, where the Graetzel solar cell is represented, a TCO glass is used as the substrate for a photoelectrode made of TiO_2 particles (size is 250-300nm) which have a good chemical stability under visible irradiation in solution.

The light passing through the TCO film is absorbed by dye molecules which are chemically bonded to the titanium oxide particles. When the light reaches the dye, an electron is transferred to the TiO_2 which carries it to the conducting glass; at the same time an electron hole is transferred from the dye through the electrolyte to the conducting glass electrode.

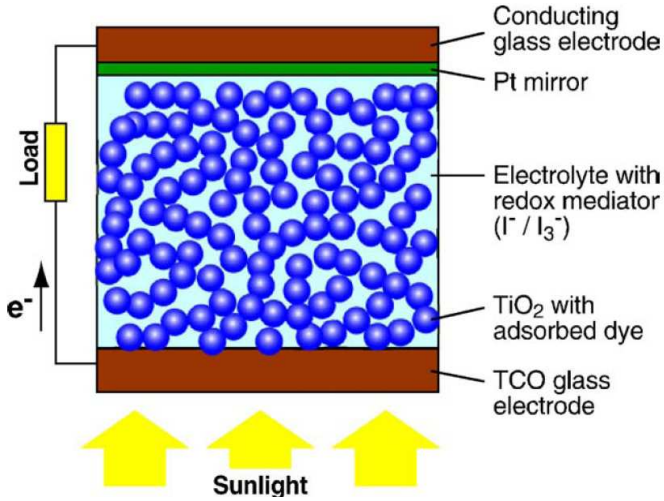

Figure 2.20: Dye-sensitized solar cell representation

This type of device has reached efficiency of 11% in its simple form [30], while a 15% for a dual-junction dye cell has been reached [31].

There are two types of problem with this technology: first the material associated with the dye is expensive today and secondly there are some issues related to the solid-liquid interface reliability in 30-year lifetimes.

Once the above problems have been solved, it seems that this technology could have good market opportunities especially because of its manufacturing low cost because there is no vacuum equipment involved.

2.2.4 Third generation

Multi-junction cells

This type of solar cells have been developed in 1980s and 1990s for the space market which required a high power to weight ratio.

The most important factor which limits the photon to electron-hole couple conversion is related to the amount of energy carried by the photon. When this energy $E_\lambda = hc/\lambda$ is greater than the material band gap E_g, the excess energy $E_\lambda - E_g$ is lost as heat. On the other hand when the photon energy is lower than the material

band gap this energy is not converted into electrical energy because the photon is not absorbed by the material.

Since the solar spectrum is broad (photons have energies in te range of about 0-4eV), the efficiency of a single-junction solar cell is significantly less than the efficiency which it could have if it received a monochromatic light.

The solution to this problem is to divide the solar spectrum into different regions and convert each energy with an appropriate cell (i.e. with the appropriate band gap). This is the idea related to the multi-junction solar cells.

The values of theoretical efficiency for multi-junction cells (with two, three, and thirty-six band gaps) have been calculated by Henry [16] and are shown in table 2.6. These efficiencies clearly indicate that if a substantial improvement using two band gaps rather than one is achieved, the returns diminish when more band gaps are added.

Number of band gaps	Efficiency [%]
1	37
2	50
3	56
36	72

Table 2.6: Theoretical multi-junction solar cell efficiencies

Figure 2.21 shows two outline of different approaches to distribuite light to solar cells having different band gaps. With reference to the left side of figure 2.21, a first way to perform the multi-junction approach is to use a prism which can distribuite photons with different energies in different places where some solar cells with different band gaps are located. This approach has some intrinsic optical and mechanical problems so that commercial multi-junction solar cells are designed in a different way.

The right side of figure 2.21, where $E_{g1} < E_{g2} < E_{g3}$, shows the customary way to split the solar spectrum. In this case photons carrying an energy greater than E_{g3} are absorbed by the first junction, photons whose energy is in the range E_{g3}-E_{g2} by the second, and, finally, the third junction converts into electrical energy the photons which carry an energy between E_{g2}-E_{g1}.

In this type of device the single junctions, that are physically separated from each other, have to be transparent in order to let the light strike the all the junction in the stack.

Figure 2.22 [4] shows different possibilities to connect a two-junction solar cell (also named *tandem* cell) to an external circuit: two, three and four terminal configurations.

Finally, figure 2.23 [4] shows a cross section of a $GaInP/GaInAs/Ge$ three-

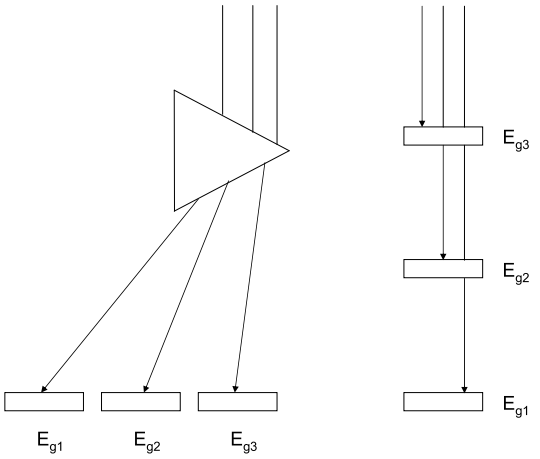

Figure 2.21: Spatial and stacked spectrum splitting

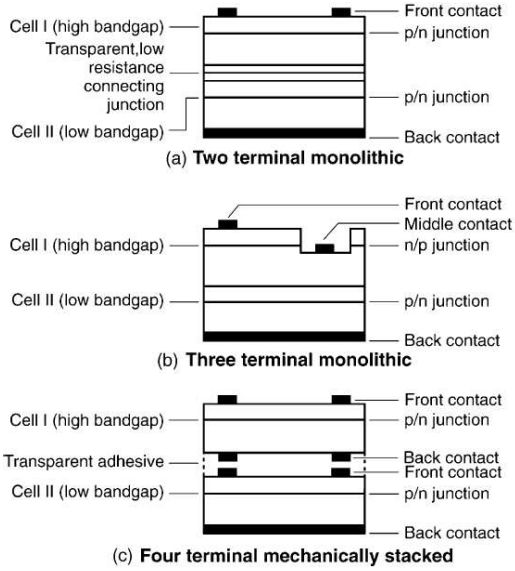

Figure 2.22: Two-junction solar cell connection possibilities

junction solar cell whose efficiency is 37.9%. Other good candidates for fabricating multi-junction solar cells are the following III-V compound semiconductors: *GaInP*/*GaAs*, *AlGaAs*/*GaAs*, *GaAs*/*GaSb*, *InP*/*GaInAs*, etc.

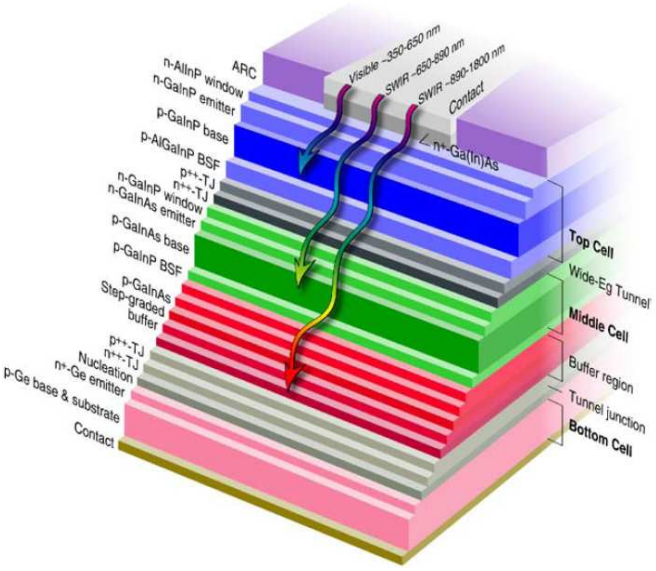

Figure 2.23: Cross-sectional representation of a three-junction solar cell

Typically the multi-junction solar cells are used, in terrestrial photovoltaic systems, in concentrator system where lenses or mirrors concentrate the sunlight (usually the direct portion) on a small photovoltaic device. The concentration ratio for *GaAs* can be as large as 1000X to 2000X (where for Si technology it can be maximum 300X).

Table 2.7 [17] shows some compound and semiconductor elements band gaps.

Compound/elements	Band gap [eV]
Si	1.12
Ge	0.7
GaInAs	1.0-1.4
AlGaAs	1.6
GaInP	1.7-1.9
AlGaInP	2.2

Table 2.7: Some compound and semiconductor elements band gaps

Intermediate band solar cells

As reported in the previous section, one of the limitations of current photovoltaic materials is the absorption of the sun's spectrum: only photons with energy higher

than the band gap can excite electrons in the conduction band (lower picture in figure 2.24).

Introducing an Intermediate Band (IB) (upper picture in figure 2.24) within the band gap enables a more efficient use of the solar spectrum. This is because below-band gap energy photons can contribute to the cell photocurrent by pumping electrons from the valence band to the intermediate band and from there to the conduction band.

It has been demonstrated that with an appropriate positioning of the intermediate band the maximum theoretical efficiency for this solar cells (also called *multi-band* cells) is 63.2% [18].

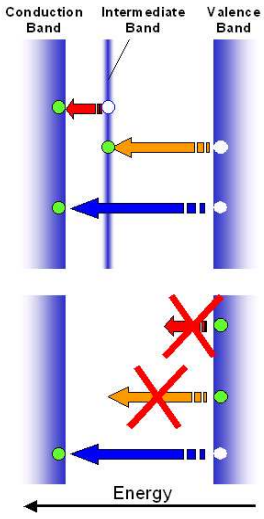

Figure 2.24: Intermediate Band concept

An intermediate band material can be obtained by embedding quantum dots (QDs) of appropriate composition and size in a matrix of semiconductor (called *host material*). Quantum dots are semi-conducting crystals of nanometer dimensions, molded into a variety of different forms with a tunable band gap of energy levels that behave as a special class of semiconductors composed of periodic groups of II-VI, III-V or IV-VI materials [19]. If the QD material is chosen so that its valence band is aligned to the valence band of the host, while there is an offset between the conduction bands, a band profile like the one depicted in the figure 2.25 is obtained.

The result, if the QDs are close enough, is a continuous electronic band within the band gap.

The idea of improving solar cells efficiencyiy by using an intermediate band was

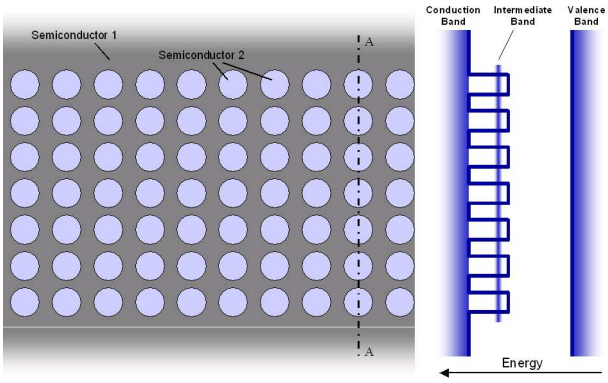

Figure 2.25: Intermediate band obtained by using QDs

born during 1960s, and, even if several research groups have been investigating structures [20-21-22], no devices using this approach have yet been validated.

Organic solar cells

Since the early 2000s the interest in organic solar cells (hereafter also called plastic solar cells) has started to grow and this is related to the development of these materials for display market.

Attractive features for plastic solar cells are the possibilities for ultra thin, flexible devices which may be integrated into appliances or building materials, and tuning of color through chemical structure [2].

The efficiencies of this devices is today near 3% [32] even if these materials can be chemically controlled to respond to different wavelengths making multiple-junction approaches a potential pathway to increased efficiencies [33].

A problem for this type of devices is that organic materials are notoriously sensitive to ultraviolet radiation that can change bonding and lead to instabilities. Higher temperature operation may also provide limitations for some organics [4].

Even if an increasing number of research groups and companies are declaring interest in this technology, organic solar cells are far away from being commercialized.

2.3 Energy payback

A photovoltaic system converts the energy carried by photons into electrical energy. This energy is obtained from a zero-cost fuel (the vast and infinite solar radiation). Moreover, power production is clean because any emission is associated with the photon electron-hole conversion.

However, the manufacturing of a photovoltaic plant needs a certain amount of energy. First for building the solar cell: energy is needed for mining, refining, and purification of the semiconductor material. Once the solar cell has been created, the production of the photovoltaic module will need more energy in order to manufacture other materials as copper (which performs the connection between the solar cells), aluminium (needed to make the photovoltaic module frame), plastic, etc. Lastly, further energy will be required in order to make the power cables, the power conditioning units, the electric boards, etc. (ref. section 3.3).

It is highly important to calculate and know the amount of energy needed to build the entire photovoltaic system: moreover, it is fundamental that this energy be lower than the energy that the system will produce during its operating life. This means that photovoltaic systems give an energy benefit to society. The *energy payback* of a photovoltaic system is the number of years required to repay the energy content of the system with its energy produced. This parameter depends on:

1. the energy required to manufacture all the photovoltaic system components
2. geometrical aspects related to the photovoltaic field which include tilt and azimut angles (ref. section 4.1.1)
3. the location of the photovoltaic system (i.e. the latitude)

Table 2.8 [1] reports a number of energy paybacks with reference to different solar cell technologies. Crystalline (c-Si) technologies have a longer energy payback because they have a much larger content of silicon than thin-film modules (ref. section 2.2.2). Shorter payback for future modules is predicted because of improved manufacturing processes and higher efficiencies.

Technology	Energy payback [years]
Current c-Si	4
Future c-Si	2
Current thin-films	3
Future thin-films	1

Table 2.8: Different technologies energy paybacks

Bibliography

[1] Luque A. and Hegedus S.: *Handbook of photovoltaic science and engineering*, Jhon Wiley and Sons Inc., 2006 , pages 41, 62, 87, 92, 93, 102, 103, 104, 310, 365, 567, 997, 998, and 999

[2] Markvart T. and Castaner L.: *Photovoltaics fundamentals and applications*, Elsevier, 2003 , pages 484, 520, 521 and 522

[3] Green M.A.: *Third generation photovoltaics*, Springer, 2006, pages 1, 2, 3, 4 and 5

[4] Kazmerski L. L.: *Solar photovoltaic R&D at the tipping point: a 2005 technology overview*, Journal of Electron Spectroscopy and Related Phenomena, Vol. 150, pages 105-135, 2006

[5] Green M., Emery K., King D. L., Hishikawa Y. and Warta W.: *Solar cell efficiency tables (version 28)*, Progress in photovoltaics: research and applications, John Wiley & Sons, Ltd 2006

[6] Slaoui A. and Collins R.T.: *Advanced inorganic materials for photovoltaics* MRS Bulletin, Vol. 32, No. 3, pages 211-214, 2007

[7] *Trends in photovoltaic applications. Survey report of selected IEA countries between 1992 and 2006*, International Energy Agency, 2006

[8] Maycock P. D., PV News, vol. 24, no. 3, PV Energy Systems, Warrenton, 2005

[9] Schmela M., Photon International: The Photovoltaic Magazine, Solar Verlag GmbH, Aachen, pages 24-35, 2005

[10] Rogol M.: *Investing in solar power: hot spots and shadows* U.S. DOE Solar Energy Technologies Review Meeting, Denver, Colorado, October 2004

[11] Zanio K.: *Cadmium Telluride* Academic Press, New York, 1975

[12] Bonnet D.: Proceedings of the 19th European Photovoltaic Solar Energy Conference-Paris, James and James, UK, pages 1657-1662, 2004

[13] Beach J. D. and McCandless B. E.: *Materials challenges for CdTe and $CuInSe_2$ photovoltaics*, MRS Bulletin, Vol. 32, No. 3, pages 225-229, 2007

[14] http://www.nrel.gov

[15] Wieting R.: American Institute of Physisc Proceedings 462, pages 3-8, 1999

[16] Henry C., Journal of Applied Physics, vol. 51, pages 4494-4500, 1980

[17] Dimroth F. and Kurtz S.: *High-efficiency multijunction solar cells* MRS Bulletin, Vol. 32, No. 3, pages 230-235, 2007

[18] Luque A. and Marti A.: *Increasing the efficiency of ideal solar cells by photon indiced transition at intermediate levels*, Physical Review Letter, Vol. 78, pages 5014-5017, 1997

[19] Manna T. K. and Mahajan S. M.: *Nanotechnology in the development of photovoltaic cells* 1-4244-0632-3/07/$20.00 ©2007 IEEE

[20] Green M.A., Cho E.C., Cho Y., Huang Y., Pink E., Trupke T., Lin A., Fangsuwannarak T., Puzzer T., Conibeer G. and Corkish R., Proceedings of the 20th European Photovoltaics Solar Energy Conference, Barcellona, 2005

[21] Wahnon P., Palacios P., Fernadez J.J. and Sanchez K., Proceedings of the 20th European Photovoltaics Solar Energy Conference, Barcellona, 2005

[22] Harder N.P., Proceedings of the 20th European Photovoltaics Solar Energy Conference, Barcellona, 2005

[23] Luque A., Marti A. and Nozik A. J.: *Solar cells based on quantum dots: multiple exciton generation and intermediate bands*, MRS Bulletin, Vol. 32, No. 3, pages 236-241, 2007

[24] Schropp R. E. I., Carius R. and Beaucarne G.: *Amorphous silicon, microcrystalline silicon, and thin-film polycristalline silicon solar cells*, MRS Bulletin, Vol. 32, No. 3, pages 219-224, 2007

[25] Duffie J. A. and Beckman W. A.: *Solar engineering and thermal processes*, Jhon Wiley and Sons Inc., 2006

[26] Cucumo M. A., Marinelli V. and Oliveti G.: *Ingegneria solare. Principi e applicazioni*, Edizioni Pitagora, 1994

[27] www.q-cells.com

[28] www.csgsolar.com

[29] Carlson D.E. and Wronsky C.R.: Applied Physics Letters, No. 28, page 671, 1976

[30] Koide N., Chiba Y., Islam A., Komiya R., Fuke N., Fukui A. and Yamanaka R., Proceedings of the 31th IEEE Photovoltaic Specialist Conference, New York, 2005

[31] Graetzel M., Proceedings of the 20th European Photovoltaics Solar Energy Conference Conference, Barcellona, 2005

[32] Brabec C.J., Sariciftci N.S. and Hummelen J.C.: *Advanced functional materials*, Plastic solar cells, Vol. 11, pages 15-26, 2001

[33] Forest S., Proceedings of the SPIE Meeting, Denver, 2003

[34] Ramanathan K., Keane J.C., To B., Dhere R.G. and Noufi R., Proceedings of the 20th European Photovoltaics Solar Energy Conference, Barcellona, 2005

Chapter 3

Photovoltaic systems

Photovoltaic systems are solar energy supply systems, which either supply power directly to electrical equipment, off grid systems, or feed energy into the public electricity grid, grid connected systems (ref. section 3.2).

The electric part of a photovoltaic system is generally made of photovoltaic modules, electronic devices, electric boards and cables.

3.1 Photovoltaic field

A photovoltaic field is made of a certain number of series and parallel connected photovoltaic modules. The aim of the section is to provide a useful method to find out the current voltage (I-V) and the power voltage (P-V) characteristics of a photovoltaic field. By using equations 3.15 and 3.19, which will be obtained in sections 3.1.2 and 3.1.3, the I-V characteristic of an arbitrary working (i.e. composed of n photovoltaic modules each one working at its cell temperature and irradiance values) photovoltaic field will be found. Finally, multiplying equation 3.15 by the current I and/or equation 3.19 by the voltage V, the photovoltaic field P-V characteristic will be found.

3.1.1 Photovoltaic module

Solar cells represent an intermediate product in the photovoltaic industry. This is because they have a limited voltage, are extremely fragile and have no mechanical support.

A photovoltaic module is made of a certain number of series connected solar cells (the series connection enables higher voltage) which are encapsulated into a robust and manageable structure. The structure guarantees an operating life of several years even under difficult environmental conditions.

The I-V characteristic of a photovoltaic module is defined by equation 2.6. However the use of equation 2.6 becomes difficult when accurate measurements of $\overline{I_{sc}}$, I_o, A, R_s, and R_{sh} (ref. section 2.1) are not provided. Commonly, instead of this parameters, a photovoltaic module data sheet reports other parameters which can be useful in order to find out the module's I-V characteristic. These parameters are:

1. the short circuit current at STC I_{sc} [A]
2. the current-temperature coefficient $\bar{z}$ [A/°C]
3. the open circuit voltage at STC V_{oc} [V]
4. the voltage-temperature coefficient $\overline{w}$ [V/°C]
5. the maximum power point current at STC I_{mp} [A]
6. the maximum power point voltage at STC V_{mp} [V]

By using these parameters an equivalent expression to 2.2 is:

$$\begin{cases} I = I_L + z(T-25) - \frac{e^{m[V+w(T-25)]}-1}{e^m-1} \\ \\ 0 \leqslant I \leqslant 1 \end{cases} \tag{3.1}$$

where I [p.u.] is the per unit current referred to I_{sc}, I_L is the per unit solar radiation referred to $1000W/m^2$, T [°C] is the cell temperature, m is an exponential factor, V [p.u.] is the per unit voltage referred to V_{oc}, z [1/°C] is the current-temperature coefficient referred to I_{sc}, and w [1/°C] is the voltage-temperature coefficient referred to V_{oc}.

The current range in equation 3.1 is due to the blocking diode (ref. section 3.1.3) which is customarily series connected to photovoltaic modules. The current-temperature coefficient z is given by:

$$z = \frac{\bar{z}}{I_{sc}} \tag{3.2}$$

while the voltage-temperature coefficient w is given by:

$$w = \frac{\overline{w}}{V_{oc}} \tag{3.3}$$

In the per unit representation of equation 3.1, the power per unit basis P_B is:

$$P_B = I_{sc} \times V_{oc} \tag{3.4}$$

The exponential factor m can be obtained by applying equations 3.1 and 3.4. From equation 2.3 the photovoltaic module fill factor is:

$$FF = \frac{V_{mp} \times I_{mp}}{V_{oc} \times I_{sc}} = \frac{P_{mp}}{P_B} \tag{3.5}$$

Multiplying equation 3.1 by voltage V, an expression of power as a function of voltage is obtained.

$$P = V\left(I_L + z(T-25) - \frac{e^{m[V+w\times(T-25)]} - 1}{e^m - 1}\right) \tag{3.6}$$

By maximizing such function, an expression of P_n is found. Then, m can be found as the value which, inserted into the P_n expression, gives the fill factor 3.5.

Equation 3.1 can also be rewritten in terms of inverse function as:

$$\begin{cases} V = \frac{1}{m} log\{[I - I_L - z(T-25)](e^m - 1) + 1\} - w(T-25) \\ 0 \leqslant V \leqslant 1 \end{cases} \tag{3.7}$$

The voltage range in 3.7 is due to the bypass diode (ref. section 3.1.3) which is customarily parallel connected to the solar cells inside the photovoltaic module.

Example

The aim of the example is to plot the I-V and P-V characteristics of a commercial photovoltaic module simply by using its data sheet. No measurements of electrical module characteristics will be needed.

The photovoltaic module used in the example is Sanyo HIP-215 NHE5 (ref. appendix B) which will be used in the University of Trieste plant. Solar cells are made of a thin mono crystalline silicon wafer surrounded by ultra-thin amorphous silicon layers (Heterojunction with Intrinsic Thin layer) [1]. The cell basic structure is shown in figure 3.1.

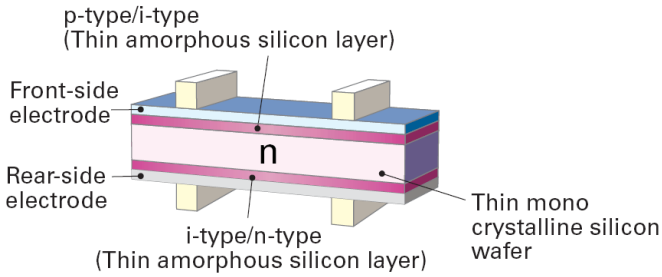

Figure 3.1: HIT technology layout

The module electrical data are reported in table 3.1 [1].

Maximum power at STC P_{mp} $[W_p]$	215
Maximum power point voltage at STC V_{mp} [V]	42.0
Maximum power point current at STC I_{mp} [A]	5.13
Open circuit voltage at STC V_{oc} [V]	51.6
Short circuit current at STC I_{sc} [A]	5.61
Voltage-temperature coefficient at STC $\overline{w}$ [V/°C]	0.129
Current-temperature coefficient at STC $\overline{z}$ [mA/°C]	1.68
Power-temperature coefficient at STC $\overline{p}$ [%/°C]	0.3
Nominal Operating Cell Temperature T_{noct} [°C]	44

Table 3.1: Sanyo HIP-215 NHE5 electrical data

From equations 3.2 and 3.3, the module voltage and current-temperature coefficients are:

$$z = \frac{0.00168}{5.61} = 2.99 \times 10^{-4} \frac{1}{^\circ C} \tag{3.8}$$

$$w = \frac{0.129}{51.6} = 2.50 \times 10^{-3} \frac{1}{^\circ C} \tag{3.9}$$

By using equation 3.5 the module fill factor is given by:

$$FF = \frac{42.0 \times 5.13}{51.6 \times 5.61} = 0.744 \tag{3.10}$$

and the exponential factor is m = 12.4.

Applying the above results to equation 3.1 the module I-V characteristic, when irradiance is 1p.u. and the solar cell temperature is 25°C, is given by:

$$I = 1 - \frac{e^{12.4V} - 1}{e^{12.4} - 1} \tag{3.11}$$

Figure 3.2 shows the HIP-215 NHE5 Sanyo I-V and P-V characteristics. The P-V characteristic has been found by multiplying equation 3.11 by voltage V.

The I-V and P-V characteristics shown in figure 3.2 are referred to STC (i.e. irradiance set to 1p.u. and cell temperature set to 25°C). For this reason the power produced at maximum power point equals the fill factor (equation 3.10) and both the short circuit current and the open circuit voltage are rated one.

Table 3.2 show the module mechanical data [1].

From equation 2.4 the STC module efficiency is:

$$\eta = \frac{42.0 \times 5.13}{1000 \times 1.57 \times 0.798} \times 100 = 17.2\% \tag{3.12}$$

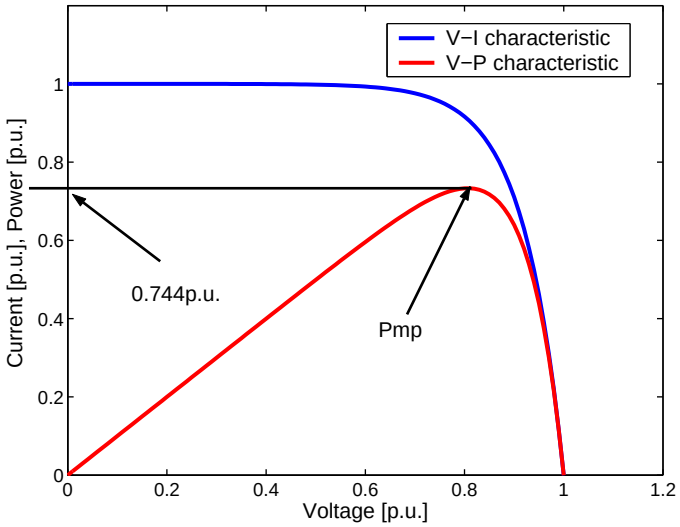

Figure 3.2: Sanyo HIP-215 NHE5 I-V and P-V characteristics

Length [mm]	1570
Width [mm]	798
Thickness [mm]	35
Weight [kg]	15

Table 3.2: Sanyo HIP-215 NHE5 mechanical data

3.1.2 Photovoltaic string

A certain number of series connected photovoltaic modules is called a photovoltaic string (figure 3.3).

The voltage across a string made of two photovoltaic modules for equation 3.7 is:

$$V_2 = \frac{1}{m} log\{[I - I_{L1} - z(T_1 - 25)](e^m - 1) + 1\} - w(T_1 - 25) \\ + \frac{1}{m} log\{[I - I_{L2} - z(T_2 - 25)](e^m - 1) + 1\} - w(T_2 - 25) \tag{3.13}$$

where $0 \leqslant V \leqslant 2$.

In equation 3.13, I_{L1} and T_1 are module number 1 solar radiation and cell temperature, while I_{L2} and T_2 are module number 2 solar radiation and cell temperature.

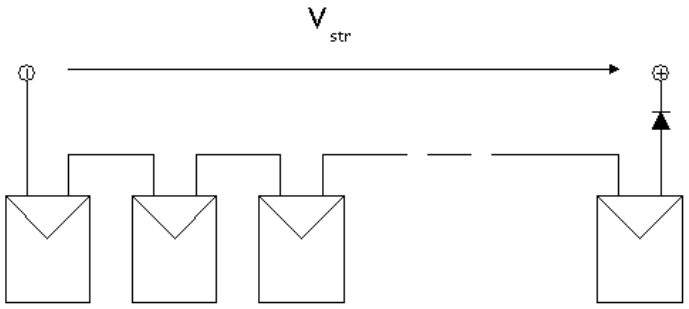

Figure 3.3: Photovoltaic string

Rearranging equation 3.13:

$$V_2 = \frac{1}{m} log\{[I - I_{L1} - z(T_1 - 25)](e^m - 1) + 1\}$$

$$\times\{[I - I_{L2} - z(T_2 - 25)](e^m - 1) + 1\}\} \tag{3.14}$$

$$-w(T_1 - 25 + T_2 - 25)$$

The I-V characteristic of n series connected photovoltaic modules for the induction principle is:

$$V_n = \frac{1}{m} log \prod_{j=1}^{n} \{[I - I_{Lj} - z(T_j - 25)](e^m - 1) + 1\}$$

$$-w \sum_{j=1}^{n} (T_j - 25) \tag{3.15}$$

where $0 \leqslant V \leqslant n$.

In equation 3.15, I_{Lj} and T_j are the j-th photovoltaic module solar radiation and cell temperature.

Example

Consider a photovoltaic string made of three Sanyo HIP-215 NHE5 photovoltaic modules (electrical parameters are described in table 3.1).

The three modules operating conditions are listed in table 3.3.

By using equation 3.15, the voltage across the string is:

$$V_3 = \frac{1}{12.4} log[(I - 1)(e^{12.4} - 1) + 1]^3 \tag{3.16}$$

	I_L [p.u.]	T [°C]
Module 1	1	25
Module 2	1	25
Module 3	1	25

Table 3.3: String operating conditions

where $0 \leqslant V \leqslant 3$.

Figure 3.4 shows the photovoltaic string I-V and P-V characteristics. The P-V characteristic has been found by multiplying equation 3.16 by current I.

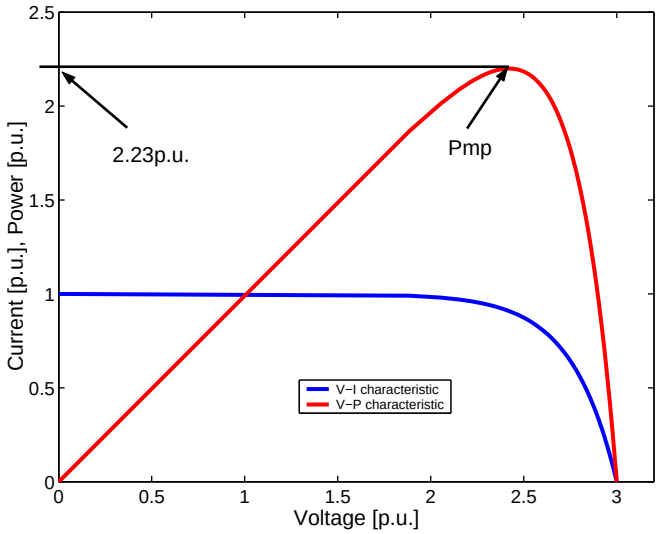

Figure 3.4: Three series connected Sanyo HIP-215 NHE5 I-V and P-V characteristics

The three series connected photovoltaic modules are working at STC. For this reason the string short circuit current is one p.u., the string open circuit voltage is three p.u., and maximum power is:

$$P_{mp} = 3 \times FF = 2.23 p.u. \tag{3.17}$$

where FF comes from equation 3.10.

3.1.3 Parallel connections

A photovoltaic field is usually made of several parallel connected photovoltaic string. This enables increased current produced and thus increased power produced.

An example of a photovoltaic field structure is reported in figure 3.5 where n photovoltaic modules are series connected to form a photovoltaic string and m photovoltaic strings are parallel connected to form a photovoltaic field.

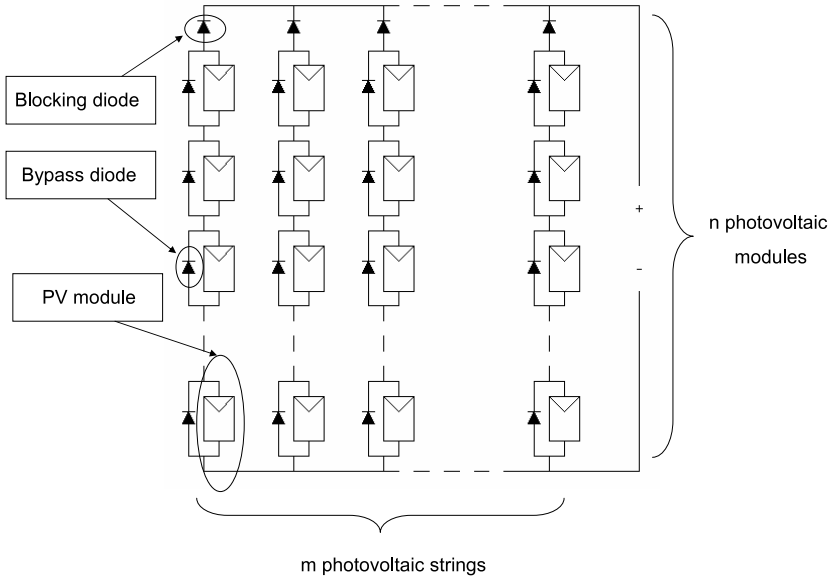

Figure 3.5: Photovoltaic field

The diode which is series connected to each string is called a *blocking diode*. In the dark a reverse current flowing through the photovoltaic string may occur; the blocking diode prevents this type of inconvenience.

The diode which is parallel connected to each photovoltaic module is called a *bypass diode*. When a photovoltaic module is being shadowed its voltage can reverse. The module reverse voltage may produce a system voltage drop and cause a power loss. Moreover, the reverse voltage causes the module to dissipate the power produced by unshaded modules and the heat can result in damage to the module (*hot spot* phenomena).

The current produced by two parallel connected photovoltaic modules, by using equation 3.1, is given by:

$$I_2 = I_{L1} + z(T_1 - 25) - \frac{e^{m[V+w(T_1-25)]}-1}{e^m-1} \\ +I_{L2} + z(T_2 - 25) - \frac{e^{m[V+w(T_2-25)]}-1}{e^m-1} \tag{3.18}$$

where $0 \leqslant I \leqslant 2$.

In equation 3.18 I_{L1} and T_1 are module number 1 solar radiation and cell temperature while I_{L2} and T_2 are module number 2 solar radiation and cell temperature.

The I-V characteristic of n parallel connected photovoltaic modules for the induction principle is:

$$I_n = \sum_{j=1}^{n} I_{Lj} + z \sum_{j=1}^{n} (T_j - 25) - \frac{1}{e^m - 1} \sum_{j=1}^{n} (e^{m[V + w(T_j - 25)]} - 1) \tag{3.19}$$

where $0 \leqslant I \leqslant n$.

In equation 3.19 I_{Lj} and T_j are the j-th photovoltaic module solar radiation and cell temperature.

Example

Consider three Sanyo HIP-215 NHE5 (electrical parameters are described in table 3.1) parallel connected modules.

The operating conditions of the three modules are the same listed in table 3.3.

By using equation 3.19, the current produced by the parallel is:

$$I_3 = 3\left(1 - \frac{e^{12.4V} - 1}{e^{12.4} - 1}\right) \tag{3.20}$$

where $0 \leqslant I \leqslant 3$.

Figure 3.6 shows the I-V and P-V characteristics for the three parallel connected photovoltaic modules. The P-V characteristic has been found by multiplying equation 3.20 by voltage V.

The three parallel connected photovoltaic modules are working at STC. For this reason in figure 3.6 the short circuit current is three p.u., the string open circuit voltage is one p.u., and maximum power is:

$$P_{mp} = 3 \times FF = 2.23 p.u. \tag{3.21}$$

where FF comes from equation 3.10.

3.2 Photovoltaic systems

Photovoltaic systems (hereafter named also photovoltaic plants) may or may not be connected to the electric grid. When a photovoltaic plant is connected to the grid, it is called *grid connected* photovoltaic plant, while otherwise it is known as an *off grid* photovoltaic plant.

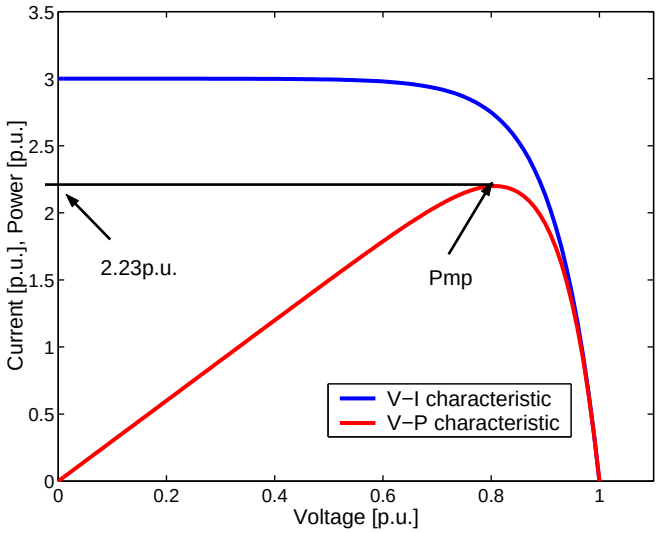

Figure 3.6: Three parallel connected Sanyo HIP-215 NHE5 I-V and P-V characteristics

3.2.1 Grid connected systems

Grid connected plants are divided into two groups: distributed and centralized plants. A functional *grid connected distributed* system block scheme is shown in figure 3.7.

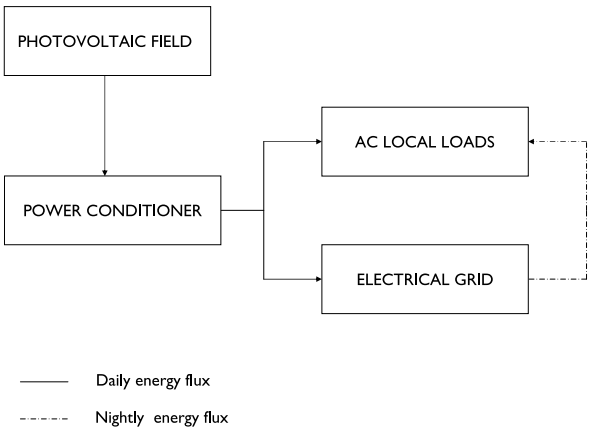

Figure 3.7: Functional grid connected distributed system block scheme

In a grid connected distributed plant the constant voltage produced by the photovoltaic field is converted into an alternate sinusoidal 50Hz voltage by a power conditioning unit (ref. section 3.3.2). These plants use the electrical grid as an ideal battery: the energy produced when the sun shines can flow either to the AC local loads or, when the energy produced exceeds the local load requirements, to the grid. On the other hand, when sun does not shine, local load requirements are covered by the grid.

This type of plants are usually located on the customer's premises in private, public and, commercial buildings. The photovoltaic systems is typically integrated as roofing, facades, shadings, etc.: this plants are known as *Building Integrated Photovoltaic* (BIPV). This type of systems is always located near cities where an electrical distribution grid (i.e. low voltage line) is present and their power limit is usually $1MW_p$.

As said previously, grid connected plants can also be centralized. A functional *grid connected centralized* system block scheme is shown in figure 3.8.

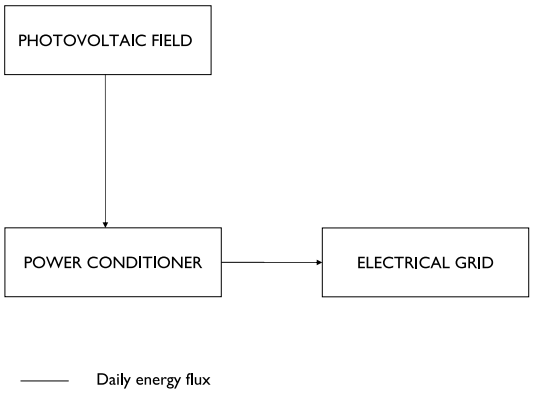

Figure 3.8: Functional grid connected centralized system block scheme

In this case the energy produced is not associated to any particular costumer and is despatched to the grid.

This type of plant performs the functions of centralized power stations, the nominal power is usually greater than $1MW_p$ and it is usually connected to the electrical transmission grid.

These systems could be located on the ground, on motorway sound barriers, and on any unused big place.

3.2.2 Off grid systems

Off grid plants are divided into two groups: domestic or non domestic (AC and DC types) plants. For both cases the photovoltaic system provides energy for lightning, refrigeration, and other low power loads when the utility electrical network is not present.

A functional *off grid domestic* system block scheme is shown in figure 3.9.

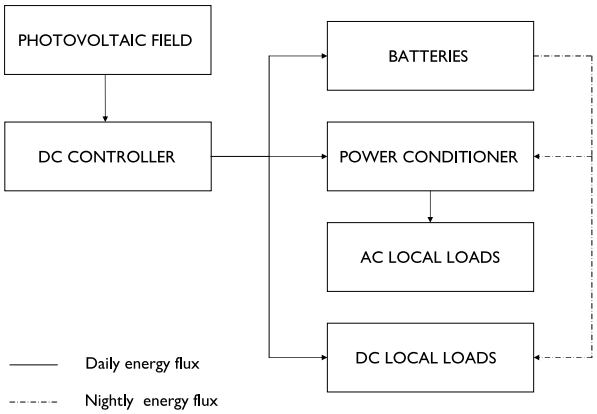

Figure 3.9: Functional off grid domestic system block scheme

The energy produced is generally used by households and villages which are not connected to an electrical grid. In a off grid domestic plant the constant voltage produced by the photovoltaic field is conditioned by a DC controller. When the sun shines, the DC current supplies directly the DC local loads or the power conditioner connected to the AC local loads. When energy produced exceeds DC and AC local load requirements, the exceeding part flows into the batteries. When the sun does not shine, the batteries directly supply DC local loads and/or supply AC local loads through the power conditioner.

This type of plant is usually located in remote villages, they are rated at maximum few kW_p and they help roughly one-third of the world's population to gain access to a modest amount of energy [2]. The photovoltaic systems could be integrated as roofing or placed on the ground.

Finally figures 3.10 and 3.11 show some functional off grid non domestic block scheme systems.

This type of plant was the first commercial application for terrestrial photovoltaic systems. They provided, and provide still today, energy for a wide range of applications, such as communications, information, water pumping, illumination,

etc. In this case the electrical loads can be both AC (ref. figure 3.10) or DC (ref. figure 3.11) and the plant rated power is usually less than $1kW_p$.

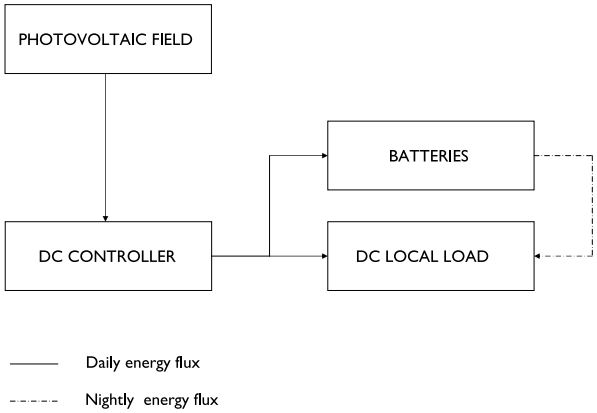

Figure 3.10: Functional off grid non domestic DC system block scheme

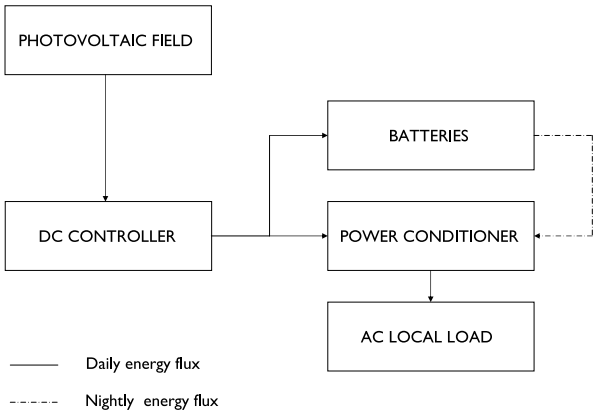

Figure 3.11: Functional off grid non domestic AC system block scheme

3.3 Electrical devices

In this section the electrical devices which, combined to the photovoltaic field, form a grid connected photovoltaic system (be it distributed or centralized) will be shortly described.

Figure 3.12 shows an electrical grid connected system block scheme. The DC current produced by the photovoltaic field is carried by DC cables through electric boards to the power conditioning units. The power conditioning units make the DC current an AC current which is delivered via AC cables to the electrical grid.

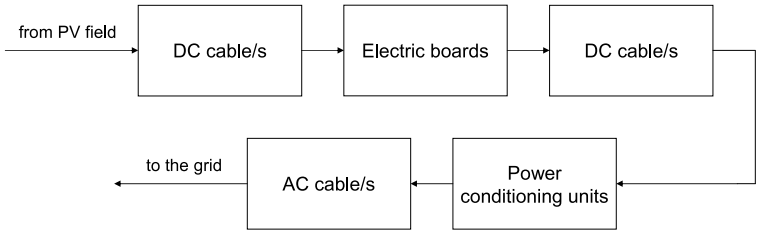

Figure 3.12: Electrical grid connected system block scheme

3.3.1 Electric boards

Direct current electric boards (DC boards) used in photovoltaic systems are generally needed in order to protect the photovoltaic strings from:

1. over currents by using fuses
2. over voltages by using surge protective devices
3. current inversions by using blocking diodes

In case of plants using a string architecture (ref. section 3.4) DC boards are usually implemented in the power conditioning unit (ref. figure 3.15). When a centralized architecture is used (ref. figure 3.16), the DC board also implements the function of paralleling the photovoltaic strings.

Alternate current electric boards (AC boards) used in photovoltaic systems implement protection relays which perform the connection to the electrical grid. They are always used in string architecture (ref. figure 3.15), while for centralized solutions the connection to the grid is usually provided by the power conditioning unit (ref. figure 3.16).

3.3.2 The power conditioning unit

The power conditioning unit (hereafter also named inverter) is the key link between the photovoltaic field and the electrical grid. It acts as an interface that converts the direct current produced by the photovoltaic modules into a utility grade current (typically alternate and sinusoidal at a frequency of 50-60Hz). The photovoltaic system behavior relies heavily on the power conditioning unit. The inverter must produce good quality sine wave output, must follow the frequency and the voltage of the grid and must extract maximum power from the photovoltaic field. This function is performed by a device known as Maximum Power Point Tracker (MPPT) [3].

Table 3.4 [4] shows a commercial power conditioning unit electrical data.

Rated photovoltaic field voltage $P_{dc,n}$ $[V]$	650
Photovoltaic field voltage range $V_{dc,range}$ [V]	430-760
Open circuit voltage $V_{dc,oc}$ [V]	880
Output voltage $V_{ac,n}$ [V]	400
Output frequency f_n [Hz]	50
European efficiency η_{eu}	94.5%
Maximum efficiency η_{max}	96.0%

Table 3.4: Elettronica Santerno TG 21 800V electrical data

The maximum power point tracker

The solar cell (module, string or field) operating point P_o, which is shown in figure 3.13, is determined by the intersection between load and solar cell characteristics.

As reported in section 2.1, there is a solar cell maximum power operating point P_{mp}. Maximum Power Point Tracker (MPPT) are devices, usually implemented in the power conditioning unit (grid connected systems) or in the DC controller (off grid systems), which continuously control power delivered by the photovoltaic generator in order to maximize it by varying the voltage. MPPT operation is continuous because I-V and P-V characteristics depend on solar radiation and solar cells working temperatures which change with time.

When the operating point is not the maximum power point some power is lost. With reference to figure 3.13, this losses can be represented by defining the MPPT efficiency as:

$$\eta_{mppt} = \frac{\int_0^t P_o(t)dt}{\int_0^t P_{mp}(t)dt} \tag{3.22}$$

where P_o is the actual power produced by the photovoltaic field under MPPT

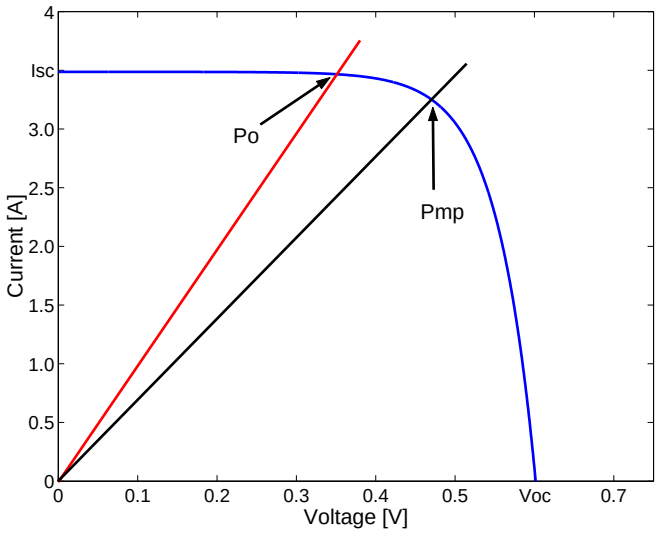

Figure 3.13: Photovoltaic field operating points

control and P_{mp} is the real maximum power the solar cell could produce under the given temperature and irradiance [5].

The MPPT function in a photovoltaic system is fundamental and its efficiency determines the cost of the photovoltaic field needed to obtain a desired power.

As said before, in grid connected photovoltaic plants MPPTs are usually implemented in the power conditioning unit. Different algorithms have been proposed for maximum power point tracking. Nevertheless, the choice of the configuration of the right converter has not been studied so widely. This exerts an important influence on the optimum performance of the photovoltaic system. MPPT methods include: incremental conductance, perturbation and observation, neural network and, curve-fitting [5]. These methods are generally implemented into DC-DC converters controller which continuously change the operating field voltage in order to follow the maximum power point. DC-DC converters commonly used for this type of applications are: buck converter, boost converter and, buck-boost converter.

Figure 3.14 shows a three series connected photovoltaic modules string P-V characteristic. Each module is working at a different climate condition with respect to the others so that the characteristic has three maximum power points: two relative (P_{r1} and P_{r2}) and one global (P_g) maximum power points. A MPPT device connected to the string would work properly only if at that instant P_g was achieved.

Commercial power conditioning units implement MPPT devices which have some problems in following P_g; it is not unusual for them to cease following the maximum power point when P_{r1} or P_{r2} is achieved. This mistake can arise at several instants during the year: the consequence could be a large amount of energy losses.

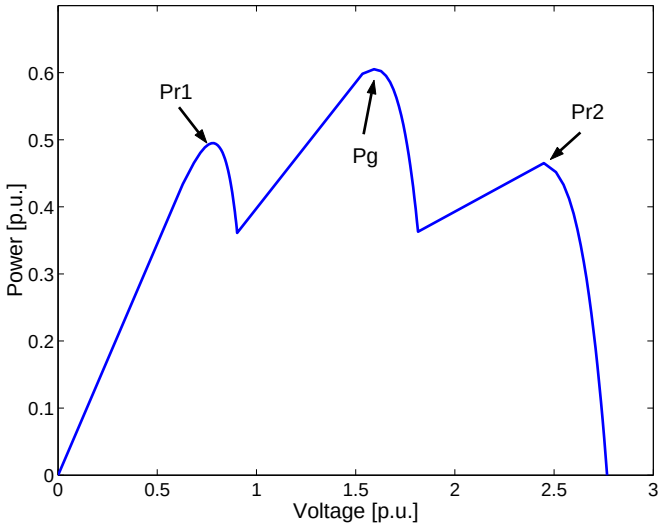

Figure 3.14: Global and local maximum power points

3.4 String and centralized architectures

From an electrical point of view, photovoltaic plants can have a string or a centralized architecture. Principle schemes of string and centralized architecture layouts are drawn in figures 3.15 and 3.16.

In a *string architecture* the number of power conditioning units is equal to the number of photovoltaic strings, while in a *centralized architecture* only one power conditioning unit is used.

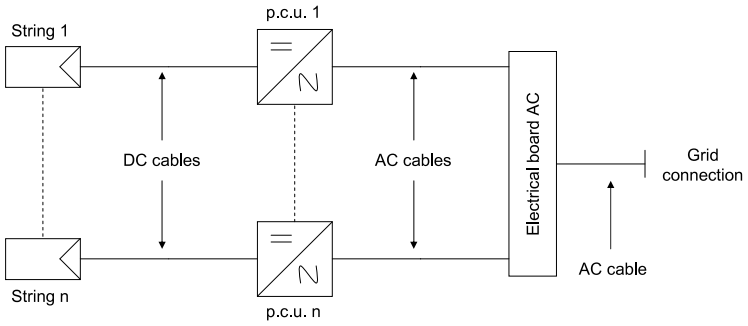

Figure 3.15: String architecture principle layout

According to the presence of one or multiple inverters, differences in the num-

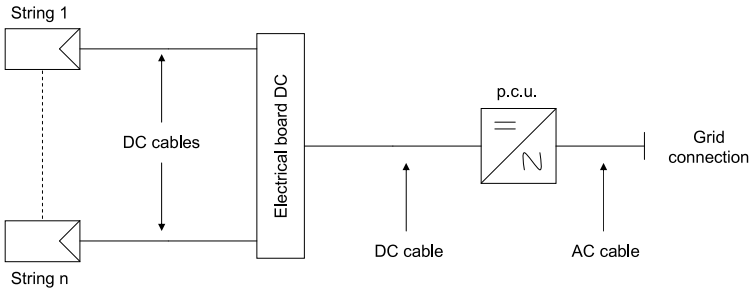

Figure 3.16: Centralized architecture principle layout

ber and type of cables (DC or AC) and connection (AC or DC electrical boards) can arise. For this reason the Balance of the System η_{bos} (ref. section 4.1) is a function of the plant architecture.

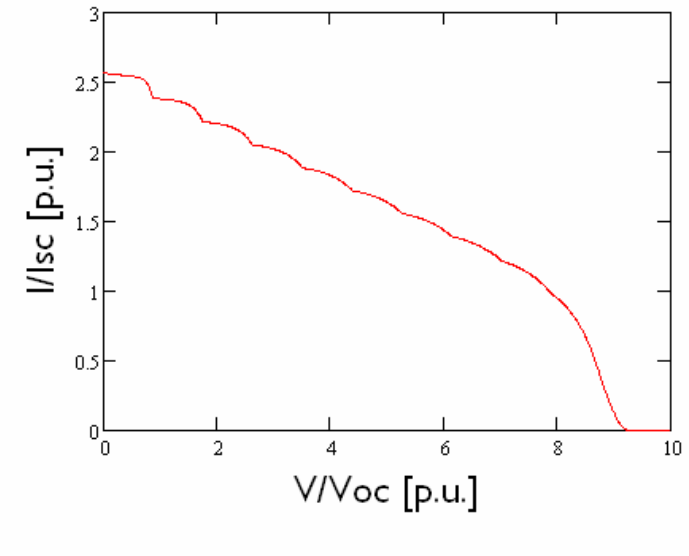

Figure 3.17: Centralized architecture I-V characteristic

Figure 3.17 [6] shows the I-V characteristic of a centralized architecture photovoltaic plant. An important issue to notice is that in this case because the strings are parallel connected, the photovoltaic field maximum power point is unique.

On the other hand, in a string architecture the number of I-V characteristics corresponds to the number of strings and the number of maximum power points

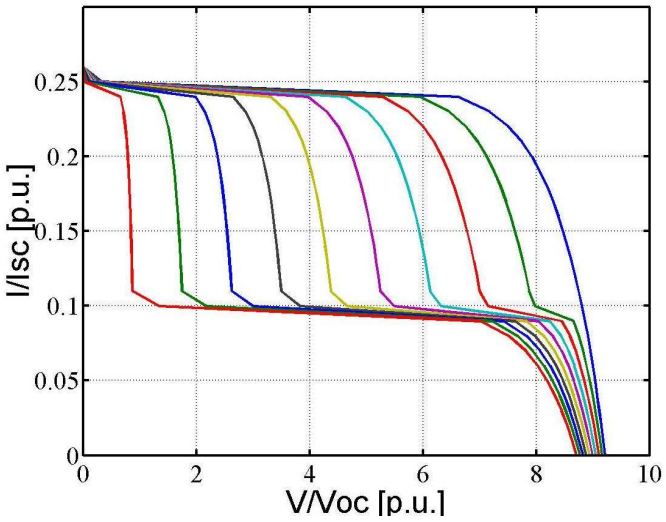

Figure 3.18: String architecture I-V characteristics

equals the number of strings, figure 3.18 [6]. In this case the photovoltaic field maximum power is the sum of the strings produced powers:

$$P_{mp} = \sum_{i=1}^{n} P_{mp,i} \tag{3.23}$$

where $P_{mp,i}$ is the the *i-th* string maximum produced power and n is the number of photovoltaic strings.

Figure 3.17 and 3.18 are representative of the same photovoltaic field made of ten strings with ten parallel connected modules. Some of these modules are shaded and some are not: table 3.5 shows the shading distribution on the photovoltaic field.

Table 3.6 shows the climate conditions adopted for shaded and for non shaded modules (this conditions are referred to the early morning of the day December 21^{st}).

As will be discussed in section 4.1.5, the choice between a centralized or a string architecture is a fundamental issue when shading phenomena along the photovoltaic field are present. From the point of view of the energy produced string architecture is always better because when a centralized architecture is used some available power may be lost. This is because the modules constituting the photovoltaic field are operated an averaged maximum power point voltage regardless of their different characteristics. The choice between the two architectures could have a different result if an economic analysis is carried out. The higher cost of smaller power conditioning systems and their lower efficiency compared to the large unique inverter used in a centralized architecture might lead the designer to choice this so-

	Number of no shaded	Number of shaded modules
String 1	10	0
String 2	9	1
String 3	8	2
String 4	7	3
String 5	6	4
String 6	5	5
String 7	4	6
String 8	3	7
String 9	2	8
String 10	1	9

Table 3.5: Shading distribution along the photovoltaic field

	No shaded modules	Shaded modules
Irradiance [p.u.]	0.25	0.1
Cell temperature [°C]	12	5

Table 3.6: Climate conditions along the photovoltaic field

lution (ref. section 4.1.5).

Example: the University of Trieste plant

The University of Trieste plant is a centralized solution example. The system is made of six strings. Each string is made of fifteen Sanyo HIP-215 NHE5 photovoltaic modules (ref. section 3.1.1). Figure 3.19 shows the overall layout of the plant.

Tables 3.7 and 3.8 report the string and the field electrical data respectively. Minimum and maximum maximum power point voltages have been calculated at -5°C and 80°C respectively.

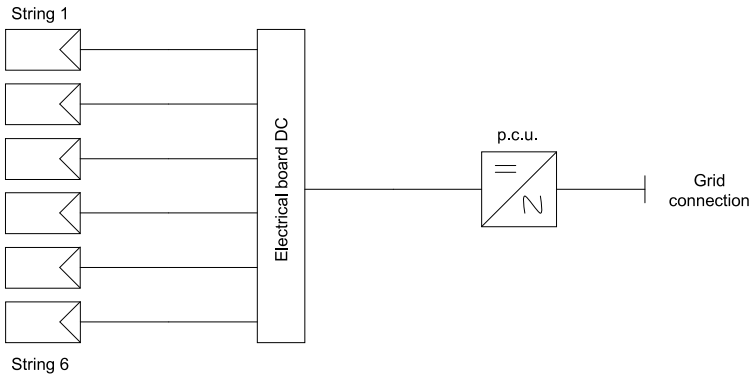

Figure 3.19: University of Trieste plant layout

Maximum power at STC P_{mp} $[W_p]$	3225
Maximum power point voltage at STC V_{mp} [V]	630
Maximum power point current at STC I_{mp} [A]	5.13
Open circuit voltage at STC V_{oc} [V]	774
Short circuit current at STC I_{sc} [A]	5.61
Lowest maximum power point voltage $V_{mp,min}$	524
Highest maximum power point voltage $V_{mp,max}$	774
Minimum open circuit voltage $V_{oc,min}$	832

Table 3.7: University of Trieste photovoltaic string electrical data

Maximum power at STC P_{mp} $[W_p]$	19350
Maximum power point voltage at STC V_{mp} [V]	630
Maximum power point current at STC I_{mp} [A]	30.8
Open circuit voltage at STC V_{oc} [V]	774
Short circuit current at STC I_{sc} [A]	33.7
Lowest maximum power point voltage $V_{mp,min}$	524
Highest maximum power point voltage $V_{mp,max}$	774
Minimum open circuit voltage $V_{oc,min}$	832

Table 3.8: University of Trieste photovoltaic field electrical data

Bibliography

[1] Sanyo HIP-215 NHE5 datasheet

[2] Luque A. and Hegedus S.: *Handbook of photovoltaic science and engineering*, Jhon Wiley and Sons Inc., 2006 , page 14

[3] Rashid M. H.: *Power electronics handbook*, Academic Press Series in Engineering, 2001

[4] Elettronica Santerno TG 21 800V datasheet

[5] Hohm D. P. and Ropp M. E.: *Comparative study of maximum power point tracking algorithms using an experimental, programmable, maximum power point tracking test bed,* 0-7803-5772-8/00/$10.00 ©2000 IEEE

[6] Massi Pavan A., Castellan S., Quaia S., Roitti S. and Sulligoi G.: *Power electronic conditioning systems for industrial photovoltaic systems: centralized or string inverters?* 1-4244-0632-3/07/$20.00 ©2007 IEEE

[7] Enrique J. M., Duran E., Sidrach-de-Cardona M. and Andujar J.M.: *Theoretical assessment of the maximum power point tracking efficiency of photovoltaic facilities with different converter topologies,* Solar Energy, Elsevier, Vol. 81, pages 31-38, 2007

Chapter 4

Energy produced

In this chapter the *Balance of System* (BOS) η_{bos} for a grid connected photovoltaic system will be defined and calculated. Once η_{bos} is known, it will be possible to calculate the energy produced by a grid connected photovoltaic plant.

4.1 The Balance of the System

With reference to figure 4.1:

1. E_{in} [kWh] is the available annual energy
2. η_{bos} is the Balance Of the System
3. E_{out} [kWh] is the annual energy delivered to the grid/AC loads

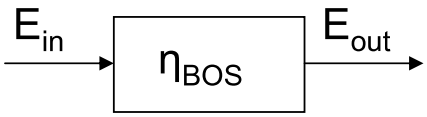

Figure 4.1: Balance Of the System (BOS)

The annual produced energy E_{out} is given by:

$$E_{out} = \eta_{bos} \times E_{in} \tag{4.1}$$

The efficiency of the system η_{bos} can be defined as:

$$\eta_{bos} = 100 - (\varepsilon_T + \varepsilon_{sha} + \varepsilon_J + \varepsilon_{mis} + \varepsilon_{pcu}) \tag{4.2}$$

where ε_T are temperature losses, ε_{sha} shading losses, ε_J Joule effect losses, ε_{mis} mismatching effect losses and, ε_{pcu} power conditioning unit losses.

4.1.1 Available energy

The available annual energy E_{in} is given by:

$$E_{in} = 365 \times G_{dm} \tag{4.3}$$

where 365 is the number of the days in a year, and G_{dm} $[kWh/kW_p \cdot day]$ is the mean global daily irradiance which depends on:

1. the particular geographic area latitude ϕ
2. the solar spectrum for the geographic area
3. the photovoltaic field tilt angle α (i.e. the angle formed by photovoltaic modules with the horizontal)
4. the photovoltaic field azimut angle γ (i.e. the azimut of the normal to the photovoltaic modules surface)
5. the ground reflectivity ε

Example

The mean global monthly irradiance for the University of Trieste plant are listed in table 4.1 [1]. The latitude is $\phi = 45.7^\circ$, the solar spectrum is AM = 1.5, the tilt angle is $\alpha = 34^\circ$, the azimut angle is $\gamma = 0^\circ$ (i.e. South direction), and the reflectivity is $\varepsilon = 22\%$ (concrete blocks).

4.1.2 Temperature losses

As discussed in section 2.1.3, the power produced by a photovoltaic module decreases when the temperature increases. The power temperature-coefficient P_{tc} in table 3.1 gives a quantity information about the losses for temperature effect compared to STC.

As an example, the losses due to temperature effect for Sanyo HIP-215 NHE5 module are given by:

$$\varepsilon_T = \overline{p} \times (T_{noct} - T_{stc}) = 0.3 \times (44 - 25) = 5.7\% \tag{4.4}$$

Month	Mean global irradiance $[kWh/kW_p \cdot day]$
January	1.82
February	2.75
March	3.72
April	4.60
May	5.44
June	5.65
July	6.35
August	6.00
September	5.12
October	3.88
November	2.27
December	1.81
Mean	4.12

Table 4.1: Mean global irradiance: Trieste location

where $\overline{p}$ is the power-temperature coefficient, T_{noct} is the Nominal Operating Cell Temperature, and T_{stc} is $25°C$ as discussed in section 2.1.2.

4.1.3 Shading losses

Shading effects along a photovoltaic field modify the value of energy which can be collected.

Figure 4.2 shows a diagram of the sun's path for Trieste (latitude $\phi = 45.7°$). Winter solstice (December 21^{st}) sun's trajectory is represented by the lower line while the highest line corresponds to the vernal equinox (March 21^{st}) sun's trajectory. In the diagram, drawn for the University of Trieste plant, the rectangle represents the shading effect due to the presence of parallel rows of photovoltaic modules (ref. appendix A).

From picture 4.2, where *A1*, *A2*, and *A3* correspond to no shaded areas while *A4* to shaded areas, it is possible to calculate the shading losses (in terms of direct irradiance) due to the presence of parallel photovoltaic modules rows during the day March 21^{st}. The shading losses are given by:

$$\varepsilon_{sha,March21^{st}} = \frac{A4}{A1+A2+A3+A4} \times 100 \tag{4.5}$$

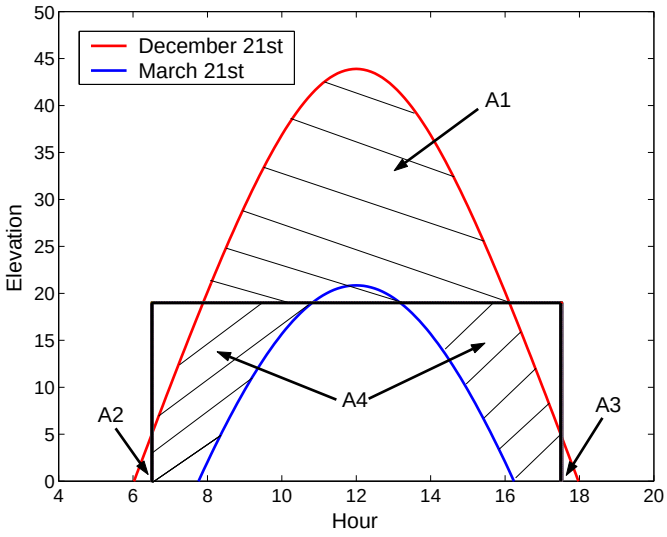

Figure 4.2: Trieste sun's path diagram

Once $\varepsilon_{sha,i}$ (i = 1, ..., 365) have been calculated for each day of the year, the annual shading losses are given by:

$$\varepsilon_{sha} = \left(\sum_{i=1}^{365} \varepsilon_{sha,i} \right) / 365 \tag{4.6}$$

where 365 is the number of the days in a year.

For the University of Trieste plant these losses are $\varepsilon_{sha} = 4.2\%$ [2].

4.1.4 Joule effect losses

As shown in figure 3.12, in a photovoltaic system DC cables link the photovoltaic field to the electric boards and thus to the power conditioning unit. Finally AC cables connect the system to the electrical grid.

In DC and AC cables some power is lost because of Joule losses which depend on cable resistance and therefore on their sections and lengths.

The losses due to Joule effect are given by:

$$\varepsilon_J = \frac{R_{dc} \times i_{dc}^2}{P_{n,dc}} + \frac{R_{ac} \times i_{ac}^2}{P_{n,ac}} \tag{4.7}$$

where i_{dc} [A] and i_{ac} [A] are the direct and the alternate currents carried by the cables connecting the different photovoltaic system components, $P_{n,dc}$ [W] and $P_{n,ac}$ [W] are the direct and the alternate currents side nominal powers, while R_{dc} [Ω] and

R_{ac} [Ω] are the direct and the alternate cables resistances which can be calculated as:

$$R = \rho \times \frac{l}{S} \tag{4.8}$$

where ρ [$\Omega mm^2/m$] is the cable resistivity calculated at an appropriate temperature and depending on the material cable, while l [m] and S [mm^2] are the cable length and section respectively.

The result for the University of Trieste plant is [2]:

$$\varepsilon_J = 0.6 + 1.8 = 2.4\% \tag{4.9}$$

4.1.5 Mismatch losses

A number of issues arise in a photovoltaic field made of several series and parallel connected modules. Mismatch losses may occur, for example, due to non uniform illumination of the photovoltaic field or because some field modules are not identical (e.g. they have different current and voltage-temperature coefficients or different fill factor, etc.). The consequence of these differences is that the output field power is different from the sum of the modules powers.

As a simple example consider two Sanyo HIP-215 NHE5 photovoltaic modules working at climate conditions described in table 4.2.

	I_L [p.u.]	T [°C]
Module 1	1	44
Module 2	0.1	20

Table 4.2: Two photovoltaic modules working conditions

The configuration using two MPPTs is shown in figure 4.3. In this case the MPPT device operates on the P-V characteristic of its photovoltaic module.

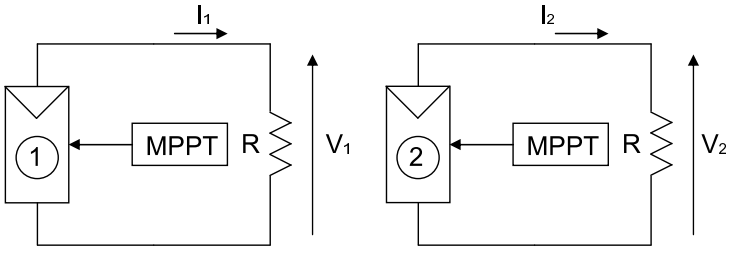

Figure 4.3: Two-MPPT electrical layout

The maximum power produced by a photovoltaic module can be easily calculated by using, for example, a Matlab M-files like:

1. m=12.4;
2. w=0.0025;
3. $I_L = 1$;
4. T=44°C;
5. V=0;
6. $while(I_L - ((exp(m \times (V + w \times (T - 25))) - 1)/(exp(m) - 1))) \times V > (I_L - ((exp(m \times (V - 0.01 + w \times (T - 25))) - 1)/(exp(m) - 1))) \times (V - 0.01)$;
7. V=V+0.01;
8. $Volt = V - 0.01$;
9. $Ampere = I_L - ((exp(m \times (V - 0.01 + w \times (T - 25))) - 1)/(exp(m) - 1))$;
10. $Watt = (I_L - ((exp(m*(V - 0.01 + w*(T - 25))) - 1)/(exp(m) - 1))) * (V - 0.01)$;
11. end;

where the exponential factor *m* and the voltage-temperature coefficient *w* have been calculated in section 3.1.1, while the current-temperature coefficient *z* has been neglected. Once the irradiance I_L and the working cell temperature T have been set, the routine starts fixing a value for the voltage (V = 0p.u. at line 5) and then increases its value until the power produced increases. When the maximum power has been reached the while loop stops and the values of current and voltage at maximum power point and the value of maximum power point are displayed.

The routine shows an ideal MPPT operation.

Table 4.3 shows the calculated power produced by the two photovoltaic modules operating at climate condition described in table 4.2 and conditioned by two MPPTs.

	Produced power [p.u.]
Module 1	0.690
Module 2	0.058
Total	0.748

Table 4.3: Produced power by using two MPPTs

Consider now the new configuration shown in figure 4.4. In this case the two photovoltaic modules are parallel connected and only one MPPT is used.

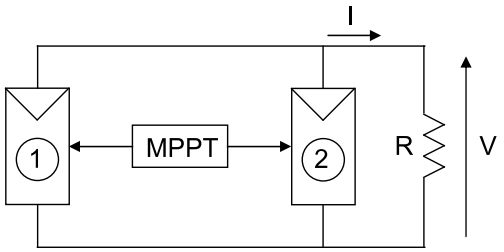

Figure 4.4: One MPPT electrical layout

The maximum power produced has been calculated by using a routine like that one shown above so that in this configuration is P = 0.730p.u.

Consequently the mismatch losses are:

$$\varepsilon_{mis} = \frac{0.748 - 0.730}{0.748} \times 100 = 2.4\% \tag{4.10}$$

These losses are due to the fact that the two photovoltaic modules are working at an averaged maximum power point regardless of their different working conditions.

The electrical architecture (ref. section 3.4) plays a fundamental role in mismatch loss determination. The two examples reported earlier show that when a centralized architecture is used (i.e. only one power conditioning unit, which corresponds to one MPPT device, is used) some power may be lost.

The value of these losses is related to shading phenomena on the photovoltaic field which always leads to different irradiance values along the photovoltaic field (which correspond to different working temperatures).

From the mismatch losses point of view the choice of a string architecture is always better. On the other hand, in a string architecture many small size power conditioning units rather than one single large one are used. The efficiency of small size power conditioning units is always less than the efficiency of a bigger machine. A further point which has to be taken into account is that the price of several small machines is higher than the price of one larger machine. However, it is clear that in order to choose the better architecture solution for a specific application, an appropriate cost benefits analysis has to be carried out (ref. section 1.4).

As explained in section 3.4, in the University of Trieste plant a centralized architecture is used. The rectangle in figure 4.2 shows the shading effect due to the presence of parallel photovoltaic modules rows. This situation leads to mismatch losses which correspond to $\varepsilon_{mis} = 2.8\%$ [2].

Finally, we should bear in mind that the mismatch losses referred to in equation 4.10 have been calculated supposing the MPPTs are working ideally. This means

that we have supposed that in every instant the MPPTs reach the global maximum power point rather than the relative one (ref. section 3.3.2). In other word we have supposed the MPPTs efficiency $\eta_{mppt} = 1$. In reality commercial MPPT efficiencies are not equal to one and this fact has to be taken into account. Unfortunately power conditioning unit data sheets don't report a value for MPPT efficiency so that the only way to take in account this phenomena is to measure it. As we will see in chapter 5, one way to measure MPPT efficiency is to use a hardware photovoltaic field simulator.

4.1.6 Power conditioning unit losses

As customary, in order to determine the considered losses take as an example the Elettronica Santerno TG 21 800V power conditioning unit; table 3.4 reports its electrical data. This table reports two values for the power conditioning unit efficiency: maximum efficiency $\eta_{max} = 96\%$ and $\eta_{eu} = 94.5\%$.

Figure 4.5 shows the Elettronica Santerno TG 21 800V power conditioning unit efficiency versus load. The plot has a maximum corresponding to η_{max} which is achieved when load is 75% of the inverter nominal load. This load depends on irradiance along the photovoltaic field. For this reason η_{max} is not sufficient to make an analysis of the energy produced in a year by a photovoltaic plant. Indeed the power conditioning unit will not work at 75% of its nominal power for most of the year. The European efficiency η_{eu} has been introduced in order to give a fuller information about the losses which occur in an inverter during a year of operations. This efficiency takes into account different regimes of operations which are a function of the photovoltaic plant installation location.

Finally, it is important to notice that both η_{max} and η_{eu} are related to the losses occurring in the power electronic devices which form the inverter such as power switches, transformers (line frequency or high frequency transformers), and so on. In reality there are other losses characterizing a power conditioning unit which are not taken into account either by η_{max} or by η_{eu} and which have to be considered. These losses are related to the way in which the inverter follows the photovoltaic field maximum power point. A power conditioning unit data sheet reports no information about these losses. Even if some information will be provided by using the simulator discussed in section 5, for the moment in order to calculate the losses occurring in the power conditioning unit, we consider its European efficiency:

$$\varepsilon_{pcu} = 100 - 94.5 = 5.5\% \tag{4.11}$$

4.2 Energy produced

In previous sections the losses in the University of Trieste plant have been discussed and calculated. By using equation 4.2, the value of the efficiency of the system is

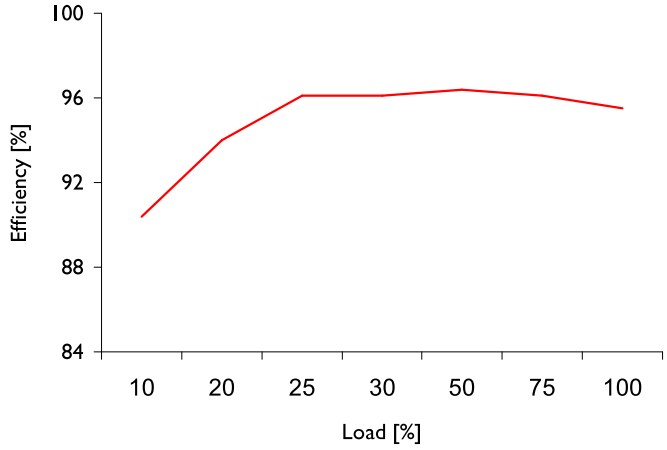

Figure 4.5: Power conditioning unit efficiency versus load

given by:

$$\eta_{bos} = 100 - (5.7 + 4.2 + 2.4 + 2.4 + 5.5) = 79.8\% \tag{4.12}$$

The annual energy on the photovoltaic plant following equation 4.3 is:

$$E_{in} = 365 \times 4.12 = 1504 kWh/year \tag{4.13}$$

where 365 is the number of the days in a year, and 4.12 is the mean global irradiance for Trieste latitude (ref. section 4.1.1).

Finally, following equations 4.1, 4.12, and 4.13, the annual energy produced by the plant is given by:

$$E_{out} = 0.798 \times 1504 = 1200 kWh/year \tag{4.14}$$

4.3 String or centralized solution?

As discussed in the example of section 3.4, the University of Trieste plant uses a centralized architecture. The aim of this section is to investigate differences between string and centralized architecture in terms of system efficiency and in terms of economic issues.

Electrical architecture	Payback period [years]
Centralized	7.4
String	8.1

Table 4.4: Comparison of payback periods

For equation 4.2, the efficiency for a photovoltaic system is given by equation 4.2:

$$\eta_{bos} = 100 - (\varepsilon_T + \varepsilon_{sha} + \varepsilon_J + \varepsilon_{mis} + \varepsilon_{pcu}) \tag{4.15}$$

where temperature ε_T and shading ε_{sha} losses do not depend on the electrical system architecture.

On the other hand, Joule ε_J, mismatching ε_{mis} and power conditioning unit ε_{pcu} losses are heavily dependent on the electrical system architecture. Assuming a hypothetical string architecture for the University of Trieste plant, the values of these losses have been calculated in work [2]. According to the calculations carried in this work, the difference in efficiency for the two solutions is $\Delta\eta_{bos} = 1.5\%$.

The better performances, due to the better efficiency and thus to higher annual productivity, achieved by the string solution have to be weighted with the different initial cost fot the two plants. A comparative economic analysis (ref. section 1.4) have been made in work [4]. With reference to the electrical equipment alone (i.e. photovoltaic modules, power conditioning unit, electric boards and cables), the results are reported in table 4.4.

Bibliography

[1] Italian regulation: *Norma UNI 10349*

[2] Massi Pavan A., Castellan S., Quaia S., Roitti S., and Sulligoi G.: *Power electronic conditioning systems for industrial photovoltaic systems: centralized or string inverters?* 1-4244-0632-3/07/$20.00 ©2007 IEEE

[3] *Photovoltaic systems. Power conditioners. Procedure for measuring efficiency*, CEI 82-20

[4] Lughi V., Massi Pavan A., Quaia S. and Sulligoi G.: *Economical analysis and innovative solutions for grid connected pv plants*. IEEE International Symposium on Power Electronics, Electrical Drives, Automation and Motion, Ischia, in press 2008

Chapter 5

The photovoltaic field simulator

Introduction

A photovoltaic field simulator (hereafter briefly called simulator) is a power electronic device which produces a current voltage characteristic that simulates the behavior of a real photovoltaic field working in arbitrary conditions of irradiance and temperature.

Once built, the simulator will be connected to the experimental photovoltaic plant which will be installed on the roof top of the Materials and Natural Resources Department at the University of Trieste.

Photovoltaic simulators are indispensable for the laboratory operational evaluation of photovoltaic energy production system components, in order to avoid time-consuming and expensive field-testing process [1].

Field testing is costly, time consuming and depends heavily on prevailing weather conditions. Adeguate security and weather protection must also be provided at the test site. To overcome these problems a photovoltaic array simulator can be used [2].

During certain period of the day/year the irradiation level is very low. It is thus difficult to test photovoltaic equipment using naturale light conditions for most of the year. If incandescent lamps are used to simulate the solar irradiation, there are problems with enormous power requirement and heat generation. Approximately 10kW of electric power is required to achieve irradiation a level of $1 kW/m^2$ for a 50W solar panel. For a 2kW solar array, the power requirement would be about 400kW! Novel discharge lamps are much more efficient. However, the spectrum does not correspond well to the sun. A further problem with solar simulators is that of achieving a uniform insolation distribution [3].

This chapter deals with the simulator description and its applications which are: photovoltaic module parameters design and power conditioning units test.

5.1 A photovoltaic simulators overview

Several types of different simulator have been proposed under different names: photovoltaic simulator, [1-4-5-6], photovoltaic array emulator [7], magnifier circuit [3], solar array simulator [8], etc. There are some particular aspects which characterized all these devices:

1. their nominal power
2. the type of control system used which can be analogue or digital. In this case the control system code could be execute by, for example, a DSP, a CPU, and so on.
3. the type of load which they can power: a resistive load, or a power conditioning unit
4. how and which parameters can be changed when the simulation is underway

The simulator nominal power P_n is an important issue because it is related with the capacity to simulate several different types of photovoltaic systems (when P_n is higher) or only photovoltaic modules or even solar cells (when P_n is lower).

The majority of simulators we have found in literature have a nominal power of a few watts [2-5-6-7-8-9]. Since the nominal power of commercial photovoltaic modules used in grid-connected applications is usually bigger than $100W_p$, these type of simulators can only simulate the behavior of few solar cells. Other works are related to more powerful simulators: 1kW [3] and 3kW [1]. These simulators can be inserted into small domestic grid-connected plants or can be used for testing/simulating only a photovoltaic string rather than the photovoltaic array of a medium/large photovoltaic plant. Tables 1.2 and 1.3 show that the larger majority of grid-connected photovoltaic plants are rated in the range 20-50kW_p. For this reason bigger simulators are needed and clearly the 20kW size could cover several applications.

A second important aspect characterizing simulators is the type of control system technology used. The versatility, reliability, velocity, and high capacity of calculus offered today by Central Processing Units (CPU) and by Digital Signal Processor (DSP) indicate that digital technology to control power electronic devices is a good choice. Most of the simulators viewed are based on an analogue control system [3-7-8], others uses as a reference the output of a real photovoltaic module [5-9]. Digital technology is used in works [1] and [2]. In the first example the control code is executed by a field-programmable gate array (FPGA) while the authors of the second work used a CPU.

Only in works [3] and [10] the simulators can be connected to a power conditioning unit while for all other cases the load was performed by a simple resistor.

The capacity to be connected to a power conditioning unit is fundamental not only for testing inverters but also for simulating the behavior of certain photovoltaic materials (in particular for thin-film technologies) working in a real photovoltaic systems.

Finally, the possibility to change the working photovoltaic modules conditions is fundamental in order to check the photovoltaic system dynamic response. For this reason simulators [5-9] which take the output of a solar cell (or even of a photovoltaic module) as their irradiance reference are not very flexible. In other simulators the climate conditions have to be set before starting the simulation [1]; in this case it is not possible to change the values of irradiance and temperatures of the photovoltaic modules while a I-V characteristic is produced. Simulators [3-6-7-8] have only the possibility to change the value of irradiance on the photovoltaic modules while the temperatures of the working modules are fixed.

The object of this work regards a simulator rated 20kW which will use a CPU technology to perform its control task. It will be possible to connect the simulator to a power conditioning unit and also change in real time values of irradiance and temperatures of the working modules.

5.2 The simulator connection scheme

Figure 5.1 shows a block scheme of a simulator which is connected to a grid connected photovoltaic plant. This block scheme is exactly the same viewed in figure 3.12 with the addition of the simulator. By closing switches A or B it is possible to power the power conditioning unit via the simulator or via the photovoltaic field respectively.

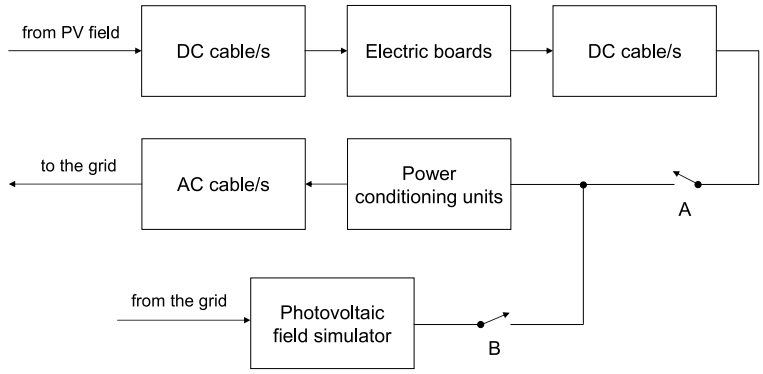

Figure 5.1: Simulator inserted in a grid connected system block scheme

The simulator is powered by an alternate sinusoidal 50Hz voltage provided by the grid and powers a power conditioning unit (figure 5.2). The I-V characteristic produced replicates the I-V characteristic of a real photovoltaic field and changes by controlling the following inputs:

1. type of photovoltaic module (ref. section 3.3.1)
2. ambient temperature
3. irradiance

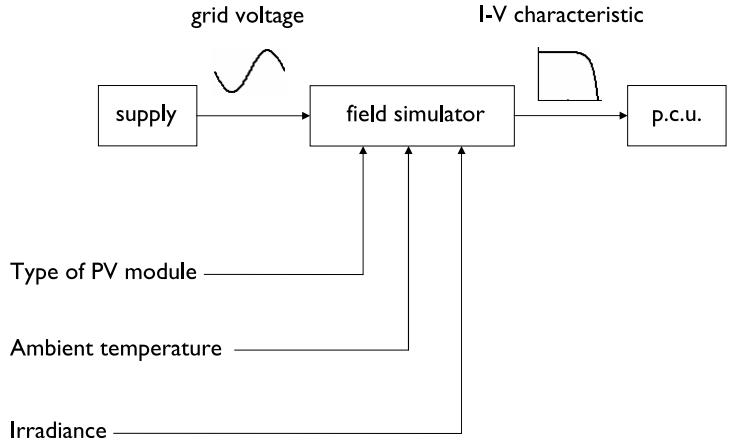

Figure 5.2: Simulator analogue output, analogue and digital inputs

Finally, table 5.1 reports the simulator electrical data:

Maximum power [kW]	20
Minimum voltage [V]	0
Maximum voltage [V]	1100
Maximum current [A]	35

Table 5.1: Simulator electrical data

5.3 The electronic power converter

As shown in figure 5.3 the simulator power hardware is made of a three phase full bridge rectifier (hereafter rectifier), a large capacitor C_1, and a step down DC-DC converter (hereafter DC-DC converter).

The rectifier converts the alternate sinusoidal 50Hz sine wave AC voltage provided by the grid V_{ac} in an uncontrolled DC voltage $V_{dc,nc}$ while the capacitor C_1 makes the DC output voltage as ripple free as possible.

The DC voltage produced by the rectifier is given by:

$$V_{dc,nc} = 1.35 \times V_{ac} \tag{5.1}$$

where $V_{dc,nc}$ stands for uncontrolled DC voltage and V_{ac} is the rms value of line to line voltage [16].

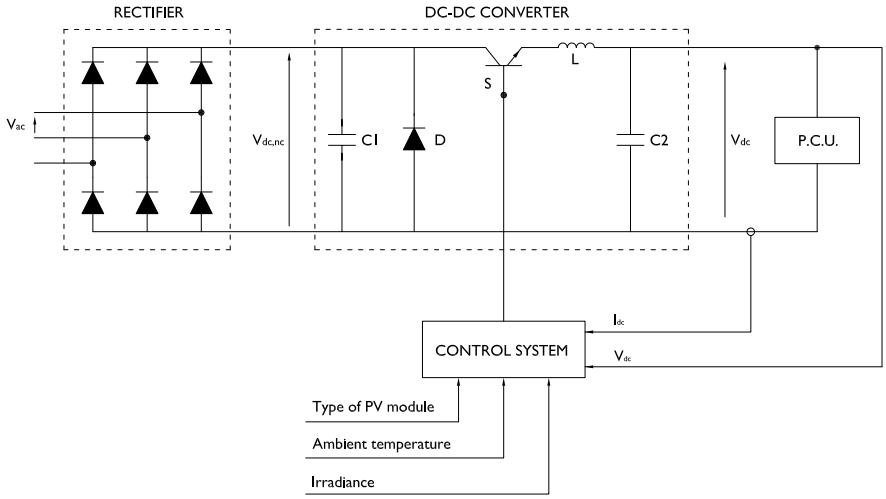

Figure 5.3: Simulator power circuit

Once the uncontrolled DC voltage $V_{dc,nc}$ has been created, the DC-DC converter converts this voltage into a controlled DC voltage V_{dc}.

The output voltage V_{dc} level is regulated by switch S on and off durations (t_{on} and t_{off}) and, with reference to figure 5.4, its value is:

$$V_{dc} = D \times V_{dc,nc} \tag{5.2}$$

where D is the switch duty ratio:

$$D = \frac{t_{on}}{T} \tag{5.3}$$

and T = $t_{on} + t_{off}$ is the constant switching time period.

One of the methods for controlling the voltage V_{dc} employs switching at a constant frequency $f = \frac{1}{T}$ and adjusting the on duration of the switch to control the average output voltage. In this method, called pulse-width modulation (PWM) switching, the switch duty ratio D is varied.

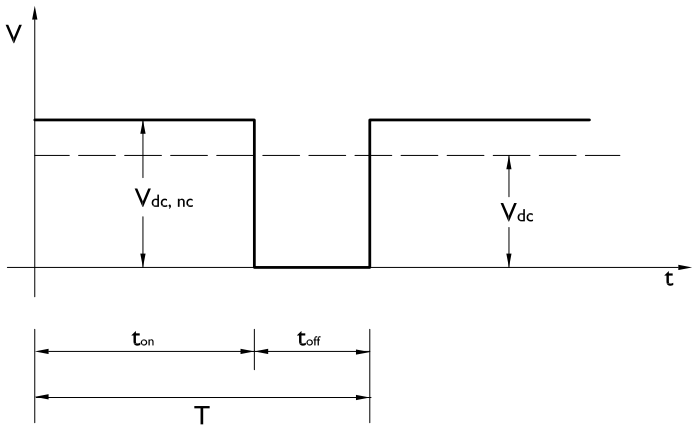

Figure 5.4: Switch mode dc-dc conversion

With reference to figure 5.5, in the PWM technique at a constant switching frequency the switch control signal is generated by comparing a control voltage, which is the difference between the desired $V_{dc,d}$ and the actual voltage $V_{dc,a}$, with a repetitive waveform. When the amplified error signal is greater than the saw-tooth waveform, the switch control signal becomes high and the switch turns on. Otherwise, the switch is off as shown in figure 5.6.

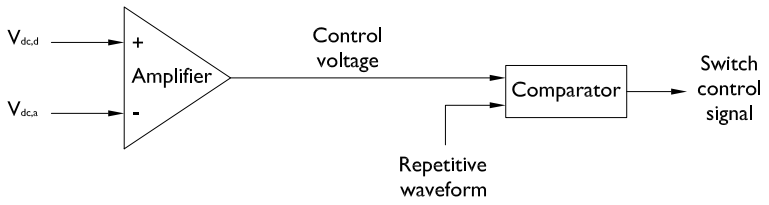

Figure 5.5: PWM block diagram

With reference to the circuit shown in figure 5.3, a real time control system generates the desired voltage signal $V_{dc,d}$ which depends on the simulation parameters: the type of photovoltaic module, the ambient temperature, the irradiance on the photovoltaic array, and the actual voltage signal $V_{dc,a}$ coming from a voltage transducer which brings the V_{dc} value. The repetitive waveform is generated since the transduced current I_{dc}.

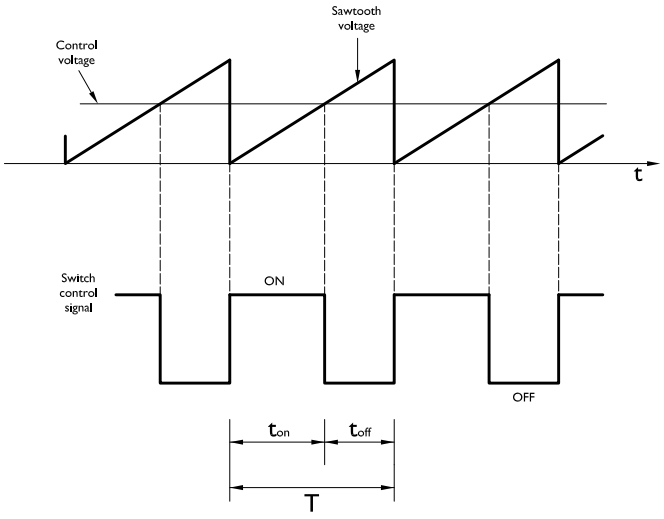

Figure 5.6: PWM signals

5.4 The real time control system

The real time control system will generate the switching signal in order to control the voltage produced by the simulator V_{dc}.

An industrialized PC-based Hard Real Time (HRT) control system based on Linux RTAI will control the switching signal by producing/managing the simulation conditions of irradiance and cells temperatures on the simulated photovoltaic field.

Normally, HRT control tasks are accomplished by employing specific dedicated CPUs, or DSPs as microcontrollers with guaranteed interrupt latency. The key issue in HRT is that the control system has to guarantee signal processing timing, without missing deadlines for interruptions and keeping latency bounded within a level compatible with the sampling time of the process [11]. In General Purpose CPUs (GPCPU), i.e. personal computers (and their industrialized versions), operative systems are mainly designed for Soft Real Time (SRT) applications (human interaction, multimedia, web browsing, office tasks, etc.). To carry out HRT controls, the Real Time Application Interface (RTAI) [12-13] will be introduced, which will make it possible to provide a HRT extension to Linux operating system [14]. This HRT extension will make it possible to utilize normal Commercial-Off-The-Shelf (COTS), low-cost personal computers, and data acquisition boards for HRT applications [15]. Furthermore, the employment of COTS personal computers will make it possible to use high level language programming tools, provided with automatic code generation. The control system model will be created using the high

level language programming *Simulink*®, which is a *Matlab*® tool for modelling, simulating, and analyzing multidomain dynamic systems. One of the advantages of this tool is that it is based on a Graphical User Interface (GUI) environment which is easy to use. Once the the control system will be created at high level, a compiler will compile a C++ code which will be loaded in a COTS endowed with Linux RTAI which will execute the code.

In general, the adoption of a COTS PC endowed with Linux RTAI gives the user some significant advantages:

1. both commercial (*Simulink*®) and free software (SCILAB) can be adopted for system modelling, simulation, and code generation
2. the savings attained from avoiding the costs of licences, proprietary software, hardware, royalties are substantial
3. RTAI is available for different hardware platforms such as PPC, Intel, ARM, etc.

5.4.1 Encoding the control software

With reference to figure 5.7, the DC-DC converter switch control signal is generated by the *Simulink*® Simulator control system block.

There are four different types of inputs:

1. inputs concerning the photovoltaic modules parameters (green lines - inputs from number 1 to number 7)
2. inputs concerning the climate data (blue lines - inputs from number 8 to number 10)
3. input concerning the control mode selection (red line - input number 11)
4. inputs concerning the external references (black lines - inputs number 12 and 13)

The first block of inputs, photovoltaic module parameters, makes it to define the photovoltaic modules which we want to simulate. The control system is provided with these parameters by the keyboard connected to the CPU which executes the code and they are:

1. the voltage-temperature coefficient w [1/°C]
2. the current-temperature coefficient z [1/°C]
3. the short circuit current at STC I_{sc} [A]

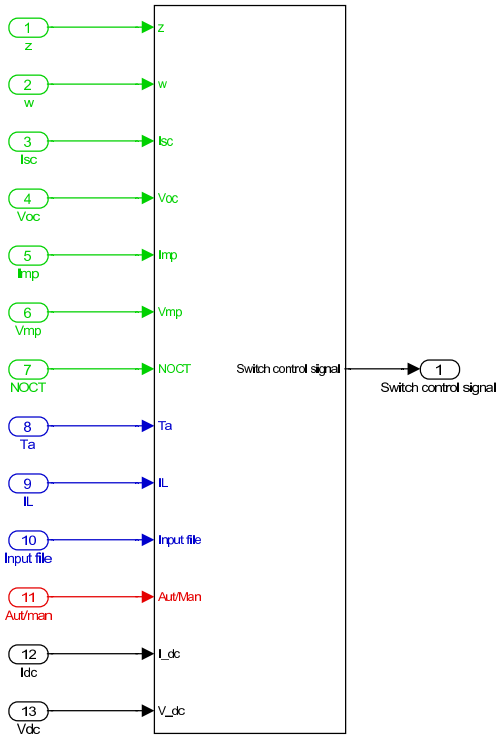

Figure 5.7: Simulator control system

4. the open circuit voltage at STC V_{oc} [V]

5. the maximum power point current at STC I_{mp} [A]

6. the maximum power point voltage V_{mp} at STC [V]

7. the Nominal Operating Cell Temperature *NOCT* [°C]

The second block of inputs defines the climate data along the photovoltaic array which we want to simulate. The ambient temperature T_a [°C] and the irradiance values I_L [p.u.] are also provided by the operator through the keyboard.

The ambient temperature T_a is a scalar while $|I_L(t)|$ is a matrix of the type:

$$|I_L(t)| = \begin{bmatrix} I_{L1}(t) \\ . \\ . \\ . \\ I_{Li}(t) \\ . \\ . \\ . \\ I_{Lm}(t) \end{bmatrix} = \begin{bmatrix} I_{L,11}(t) & I_{L,12}(t) & \dots & I_{L,1n}(t) \\ . & & & \\ . & . & & \\ . & & & \\ . & & I_{L,ij}(t) & \\ . & & & \\ . & & & . \\ . & & & \\ I_{L,m1}(t) & & & I_{L,mn}(t) \end{bmatrix} \tag{5.4}$$

where m is the number of photovoltaic strings in the photovoltaic array and n is the number of photovoltaic modules forming a string so that the vector $\bar{I}_{Li}(t)$ represents the irradiance related to the *i-th* string and the element $I_{L,ij}(t)$ represents the irradiance in the *j-th* photovoltaic module inserted in the *i-th* string.

The climate conditions can also be automatically created by the control system when the automatic mode is selected via keyboard (third input).

Finally, the fourth input block concerns the external references I_{dc} and V_{dc} which close the two control loops (as shown in figure 5.3). The control systems receives these inputs from two hardware transducers.

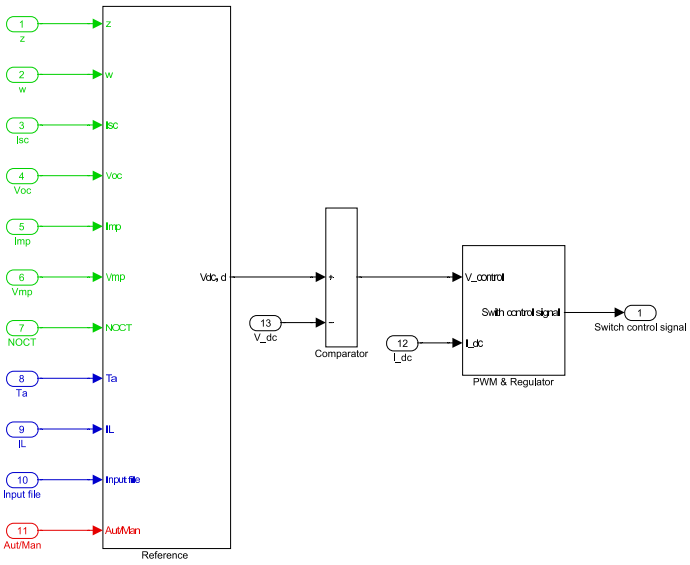

Figure 5.8: Switch control signal generation

Figure 5.8 shows the way in which the switch control signal is generated. The switch control signal is generated by the *PWM and Regulator block* which regulates

and compares its inputs $v_{control}$ and I_{dc} which represents the repetitive waveform seen in figure 5.6.

The control voltage has been calculated as the difference between the desired voltage reference $V_{dc,d}$ and the actual voltage V_{dc} as shown in figure 5.5.

Finally, figure 5.9 shows how the control voltage $V_{dc,d}$ is generated. The *PV Array block* implements equation 3.15 which make it possible to calculate the voltage across a photovoltaic string made of *n* photovoltaic modules. Also equation 3.19 is implemented in the PV Array block so that the current produced by a photovoltaic field made of *m* photovoltaic strings is calculated.

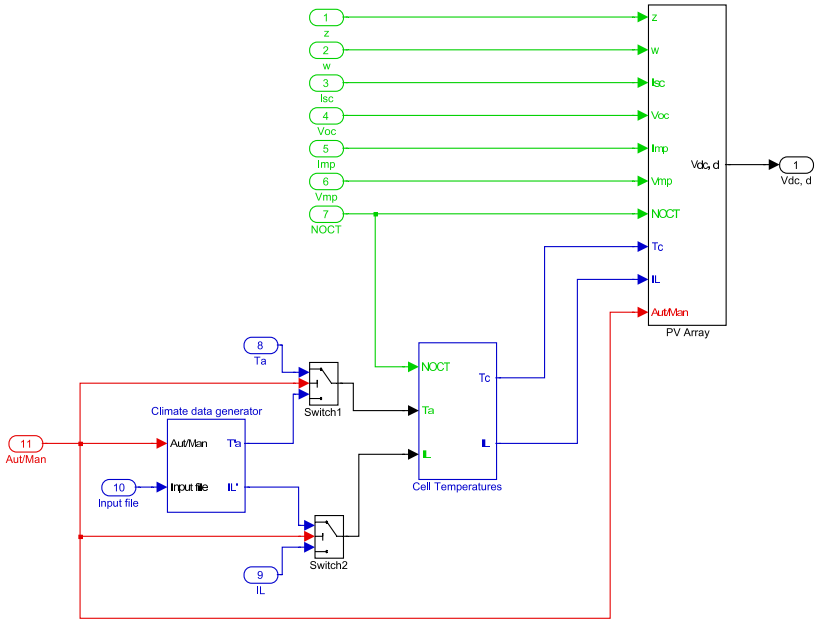

Figure 5.9: Voltage reference generation

By using equations 3.15 and 3.19 the string voltage (i.e. the field voltage) and the field current are calculated from the ambient temperature and the irradiance matrix discussed in equation 5.4. These values can be loaded by an operator via keyboard or, when the automatic mode is set, the *climate data generator* generates the time dependent climate conditions $I_L^{'}(t)$ and $T_a^{'}(t)$. An input file makes it possible to choose different ways to perform a test on photovoltaic systems. Example of input files could be:

1. a file containing a set of climate conditions during a due day in order to simulate the daily behavior of a photovoltaic system

2. a file containing a set of climate conditions during particular periods of the

year. For example during a period characterized by shading conditions along the photovoltaic field in order to simulate the shaded condition behavior of a photovoltaic system

3. etc.

The elements $T_{c,ij}(t)$ of the time dependent solar cells temperatures matrix $|T_c| = |T_c(t)|$:

$$|T_c(t)| = \begin{bmatrix} T_{c1}(t) \\ . \\ . \\ . \\ T_{ci}(t) \\ . \\ . \\ . \\ T_{cm}(t) \end{bmatrix} = \begin{bmatrix} T_{c,11}(t) & T_{c,12}(t) & \dots & T_{c,1n}(t) \\ . & & & \\ . & . & & \\ . & & & \\ . & & T_{c,ij}(t) & \\ . & & & \\ . & & & . \\ . & & & \\ T_{c,m1}(t) & & & T_{c,mn}(t) \end{bmatrix} \tag{5.5}$$

are calculated by the *Cell Temperatures block* by using equation 2.9 in a per unit notation:

$$T_{c,ij}(t) = T_a(t) + I_L(t) \times (NOCT - 25) \tag{5.6}$$

where $T_{c,ij}(t)$ is the irradiance investing the *j-th* photovoltaic module inserted in the *i-th* string, $T_a(t)$ is the ambient temperature, and *NOCT* is the value of the Nominal Operating Cell Temperature.

In equation 5.5, the vector $\overline{T}_{ci}(t)$ represents the cell temperatures related to the i-th string and the element $T_{c,ij}(t)$ represents the cell temperature of the j-th photovoltaic module inserted in the i-th string.

5.5 Photovoltaic module parameters investigation

The simulator will be useful in order to foresee the behavior of new photovoltaic devices operating in real grid connected photovoltaic systems before building them. An hardware simulation (rather than the widely used software simulation) is necessary since, while the electric model of a new solar cell can be known, the MPPT device (which is implemented in the power conditioning unit) model is not. Thus the only way to test a solar cell working near its maximum power point is to use a hardware simulator as that one discussed in this section.

For the above reason, the simulator could become a useful tool for materials engineers during design of new photovoltaic devices (i.e. when they are working

on solar cell exponential factor, voltage and current-temperature coefficients, short circuit current, open circuit voltage, fill factor, and so on).

The operation of a MPPT device has a particular relevance for the application of thin-film photovoltaic technology. This is because for this technology the maximum power operating point varies considerably with temperature and irradiance. The maximum power point changes both in the value of maximum power and in the value of maximum power voltage.

As an example, consider a monocrystalline silicon (hereafter Si) and a thin-film cadmium telluride photovoltaic (hereafter CdTe) module whose electrical data are listed in tables 5.2 and 5.3 [17-18] (ref. appendix B).

Maximum power at STC P_{mp} $[W_p]$	180
Maximum power point voltage at STC V_{mp} [V]	37.2
Maximum power point current at STC I_{mp} [A]	4.8
Open circuit voltage at STC V_{oc} [V]	44.4
Short circuit current at STC I_{sc} [A]	5.2
Voltage-temperature coefficient at STC $\overline{w}$ [V/°C]	0.16
Nominal Operating Cell Temperature T_{noct} [°C]	48

Table 5.2: Solterra 180H electrical data

Maximum power at STC P_{mp} $[W_p]$	55
Maximum power point voltage at STC V_{mp} [V]	60.0
Maximum power point current at STC I_{mp} [A]	0.92
Open circuit voltage at STC V_{oc} [V]	88.0
Short circuit current at STC I_{sc} [A]	1.09
Voltage-temperature coefficient at STC $\overline{w}$ [V/°C]	0.22
Nominal Operating Cell Temperature T_{noct} [°C]	45

Table 5.3: First solar FS-55 electrical data

By using the equations given in section 3.1.1, the exponential factor and the voltage-temperature coefficient for these modules have been calculated as: m_{Si} = 15.8 and m_{CdTe} = 5.7, w_{Si} = 0.0036/°C and w_{CdTe} = 0.0022/°C. The current-temperature coefficients have not been calculated because they will be neglected in the following discussion.

In order to show the maximum power point climate conditions dependance consider two different operating points. The irradiance values I_L of these two points are reported in table 5.4; they are the same for both technologies. The corresponding cell temperatures have been calculated by applying equation 2.9 considering an ambient temperature set at 20°C.

Technology	I_L [p.u.]	P [p.u.]	V [p.u.]
Si	1.0	0.71	0.77
Si	0.5	0.36	0.77
CdTe	1.0	0.55	0.69
CdTe	0.5	0.24	0.61

Table 5.4: Si and CdTe operating points

The third and fourth columns of table 5.3 report the produced powers P and the maximum power voltages V respectively. For both technologies a decrease in irradiance from 1.0 to 0.5p.u. has been considered. The corresponding change in produced power and maximum power voltage for Silicon technology are:

$$\frac{\Delta P_{Si}}{P} = \frac{P_1 - P_2}{P_1} = \frac{0.71 - 0.36}{0.71} \times 100 = 49\% \tag{5.7}$$

$$\frac{\Delta V_{Si}}{V} = \frac{V_1 - V_2}{V_1} = \frac{0.77 - 0.77}{0.77} \times 100 = 0\% \tag{5.8}$$

Similarly, for the Cadmium Telluride technology these variations are:

$$\frac{\Delta P_{CdTe}}{P} = \frac{P_1 - P_2}{P_1} = \frac{0.55 - 0.24}{0.55} \times 100 = 56\% \tag{5.9}$$

$$\frac{\Delta V_{CdTe}}{V} = \frac{V_1 - V_2}{V_1} = \frac{0.69 - 0.61}{0.69} \times 100 = 12\% \tag{5.10}$$

Equations 5.7 and 5.9 indicate that, given same change in irradiance values ($\Delta I_L = 0.5 p.u.$), the corresponding change in produced power is greater for CdTe than Si technology (56% versus 49%). Moreover, equations 5.8 and 5.10 show that the change in maximum power voltage is zero for Si technology and 12% for CdTe technology.

The situation is clearly shown in figure 5.10 where the P-V characteristics for the two technologies have been drawn (continuous lines show the P-V characteristics of Si technology while the dotted lines show the P-V characteristics of CdTe technology). In the plot points A and B, which correspond to Si technology, are parallel to the power axis while points C and D, which correspond to CdTe technology, are not.

From the point of view of following the maximum power point, the above discussion shows that a change in irradiance leads to greater problems when a thin-film (in this case CdTe) rather than a crystalline technology is used.

The hypothesis assumed for the irradiance change (which has been moved from 1.0 to 0.5p.u.) takes into account real situations when a rapid shading effect on the photovoltaic field occurs.

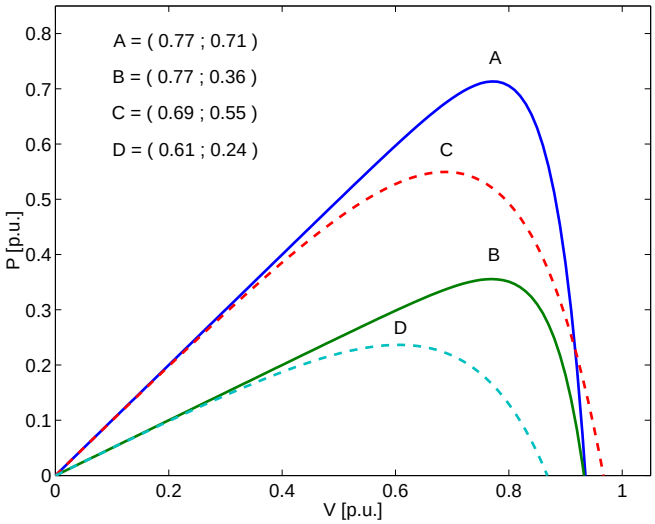

Figure 5.10: Si and CdTe photovoltaic modules P-V characteristics

There is a similar dependance of the maximum power point on temperature. However, the time constants involved in temperature changes are quite long to create problems for MPPT devices.

Finally, it is important to note that the different behavior between crystalline and thin-film technology is related to their different solar cell fill factors. Crystalline solar cells have higher fill factors than thin-film cells. This means that the maximum power point is closer to the open circuit voltage than for thin-film solar cells. This is shown in figure 5.11 where the I-V characteristic for a Si and a CdTe photovoltaic modules have been drawn.

In addition, thin-film solar cells have markedly different fill factors for different levels of solar radiation. This means that thin-film solar cells stand to benefit significantly from accurate maximum power point tracking.

5.6 Power conditioning units investigation

There are several useful tests which can be performed while checking a power conditioning unit. For these tests consider figure 5.12 where a power analyzer has been inserted in order to measure DC (P_{in}) and AC (P_{out}) powers. The analyzer will also provide the DC and AC voltages and currents values.

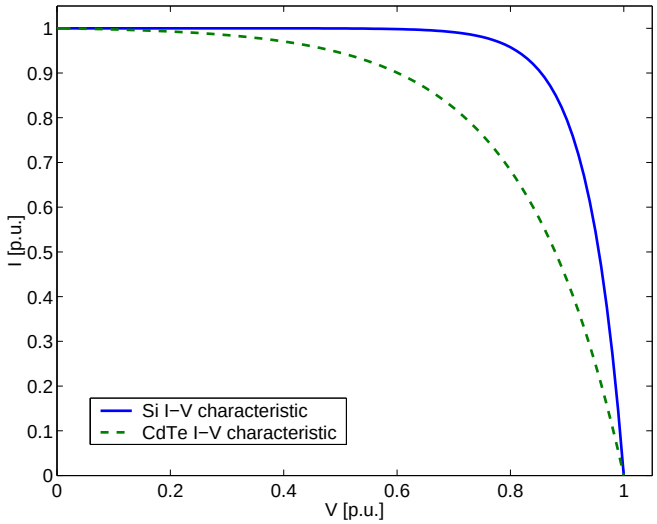

Figure 5.11: Si and CdTe I-V characteristics

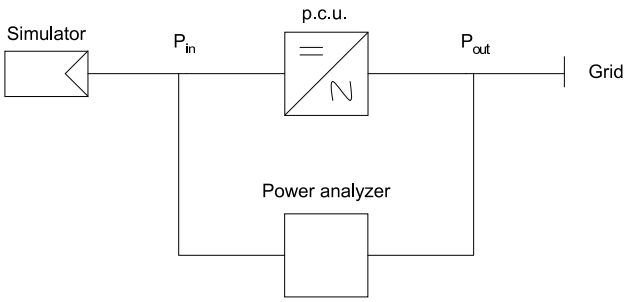

Figure 5.12: Measure system insertion scheme

5.6.1 Static efficiency

As discussed in section 4.1.6, a power conditioning unit is characterized by a maximum efficiency η_{max}. This efficiency is due to the losses in the inverter components (switches, transformers, etc.). In order to validate the value of the maximum efficiency, the power conditioning unit must be made to work at the load declared in the inverter data sheet for which η_{max} occurs. Hence, with reference to figure 5.12, the value of maximum efficiency will be:

$$\eta_{max} = \frac{P_{out}}{P_{in}} \tag{5.11}$$

As discussed in section 4.1.6, for most of the year the power conditioning unit will not work at a load corresponding to η_{max}. For this reason, the European efficiency η_{eu} has been introduced in order to give fuller information about the losses which can occur in an inverter during a year of operations. This value of efficiency takes into account different regimes of operations which are related to the latitude where the photovoltaic plant is installed. One problem is that inverter data sheets report a η_{eu} value related to higher latitude than the Italian (i.e. German latitude). The simulator will be useful in order to determine a more significant value of efficiency for Italian and other latitudes.

5.6.2 Dynamic losses

A second test which can be performed on a power conditioning unit regards its MPPT device behavior. The use of a simulator for which the temperature and the irradiance can be supplied as time sequences is the only way to test the operation of an MPPT device. This is because, as discussed in section 4.1.5, the information about MPPT device is not reported in a power conditioning unit data sheet.

Furthermore, a method involving a simulator has the major advantage of providing a repeatable test that can be used to ascertain figures for various aspect of the MPPT's performance.

In order to perform good tests, it is important to choose hard working conditions for the inverter such as when it is powered by an I-V characteristic produced by a virtual photovoltaic field where many modules are working at different climate conditions (for example due to shading phenomena on the photovoltaic field).

The simulator will be able to simulate the I-V characteristics produced during a year by a photovoltaic field for which some shading phenomena occurs by using appropriate climate input files (ref. section 5.4.1).

The capacity of the inverter in following the maximum power point during all the year will then be expressed by:

$$\eta_{mppt} = \frac{\int_0^t P_{in}(t)dt}{\int_0^t P_{mp}(t)dt} \tag{5.12}$$

where P_{in} is the inverter power input and P_{mp} is the maximum power which can be produced at that instant by the simulator. Power P_{in} will be read instant by instant by the power analyzer shown in figure 5.12, while power P_{mp} will be known when the climate data input file is set.

5.6.3 Voltage range

As reported in table 3.4, a power conditioning unit is characterized by an MPPT working voltage window: in the case of the Elettronica Santerno TG 21 800V inverter, this range is [430-760V]. This means that when the photovoltaic field voltage can not reach the minimum value 430V (i.e. because the temperature of the working photovoltaic modules is too high, ref. section 2.1.3) or when the field voltage can not be smaller than the maximum value 760V (i.e. because the temperature of the working photovoltaic modules is too low, ref. section 2.1.3), the power conditioning unit takes out the photovoltaic field and no energy is converted.

The use of the simulator will enable tests on the lower and on the higher limits of the MPPT window, especially in order to check the power conditioning unit dynamic response near these critical points.

5.7 The simulator and the plant

In figure 5.13 the insertion of the simulator in the University of Trieste plant electrical circuit is shown. As discussed in section 5.2, a switch selects alternatively the photovoltaic field (via a DC board) or the simulator as the power input for the power conditioning unit.

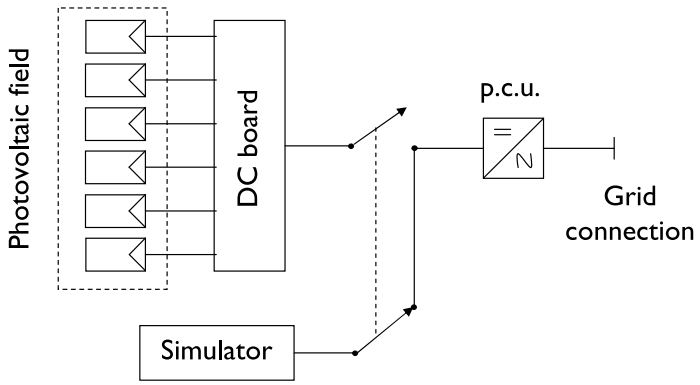

Figure 5.13: Simulator inserted in the University of Trieste plant

Bibliography

[1] Koutroulis E., Kalaitzakis K. and Tzitzilonis V.: *Development of an FPGA-based system for real time simulation of photovoltaic modules,* 0-7695-2580-6/06/$20.00 ©2006 IEEE

[2] Khouzam K., Ly C., Koh C.K. and Ng P.Y.: *Simulation and real-time modelling of space photovoltaic systems,* CH3365-4/94/0000-2038$4.00 ©1994 IEEE

[3] Olilla J.: *A medium power PV-array simulator with a robust control strategy,* 0-7803-2550-8/95/$4.00 ©1995 IEEE

[4] Nagayoshi H. and Atesh M.: *Partial shading effect emulation using multi small scale module simulator units,* 0-7803-8707-4/05/$20.00 ©2005 IEEE

[5] Park M. and Yu I. K.: *A novel real time simulation technique of photovoltaic generation systems using RTDS,* 0885-8969/04$20.00 ©2004 IEEE

[6] Zeng Q., Song. P. and Chang L.: *A photovoltaic simulator based on DC chopper,* 0-7803-7514-9/02/$17.00 ©2002 IEEE

[7] Nagayoshi H.: *Characterization of the module/array simulator using I-V magnifier circuit of a pn photo-sensor,* 3rd World Conference on Photovoltaic Energy Conversion, Osaka, 2003

[8] Lopes L. A. C. and Lienhardt A. M.: *A simplified nonlinear power source for simulating PV panels,* 0-7803-7754-0/03/$17.00 ©2003 IEEE

[9] Nagayoshi H., Orio S., Kono Y. and Nakajima H.: *Novel PV array/module I-V curve simulator circuit,* 0-7803-7471-1/02/$17.00 ©2002 IEEE

[10] Lloyd S. H., Smith G. A. and Infield D. G.: *Design and construction of a modular electronic photo-voltaic simulator,* Power Electronics and Variable Speed Drives, Conference Pubblication No. 475 ©2004 IEEE

[11] Chiandone M., Cleva S., Menis R. and Sulligoi G.: *Industrial motion control applications using Linux RTAI,* Proceedings of the 19th IEEE International

Symposium on Power Electronics, Electrical Drives, Automation and Motion, Ischia, in press 2008

[12] http://www.aero.polimi.it/rtai/

[13] http://www.rtai.org

[14] http://www.kernel.org

[15] Dozio L. and Mantegazza P.: *Real time distributed control systems using RTAI*, Proceedings of the 6th IEEE International Symposium on Object-Oriented Real-Time Distributed Computing, ISORC, 2003

[16] Mohan N., Undeland T. M. and Robbins W. P.: *Power electronics*, John Wiley & Sons, Inc., 1995, pages 161, 162, 163, 164, 165, 166 and 167

[17] Solterra 180H datasheet

[18] First solar FS-55 datasheet

[19] Altas I. H. and Sharaf A. M.: *A photovoltaic array simulation model for Matlab-Simulink GUI environment*, 1-4244-0632-3/07/$20.00 ©2007 IEEE

[20] Karatepe E., Boztepe M. and Colak M.: *Development af a suitable model for characterizing photovoltaic arrays with shaded solar cells*, Solar Energy, Elsevier, Vol. 81, pages 977-992, 2007

[21] De Soto W., Klein S. A., Beckman W.A.: *Improvement and validation of a model for photovoltaic array performance*, Solar Energy, Elsevier, Vol. 80, pages 78-88, 2006

[22] Phani Kiranmai K. S. and Veerachary M.: *Maximum power point tracking: a PSPICE circuit simulator approach*, 0-7803-9296-5/05/$20.0O ©2005 IEEE

Conclusions

Following an introduction regarding photovoltaic systems, which includes the state of the art technology and some economic issues (in order to make a comparison between different photovoltaic systems), some basic concepts on solar cells and a brief technologies and materials review has been given. The classic model of a solar cell has been explained and the electrical characteristics of a solar cell have been mentioned. The technology and materials review has been made considering the classification proposed by Martin Green. He identifies a first generation of solar cells including silicon both single and multi crystalline wafers (c-Si), a second regarding thin-film based solar cells (a-Si, CIS, CdTe, etc.), and finally, a third which comprises multijunction, multi band, intermediate band, organic solar cells, etc.

Moving on from the above basic concepts, this work presents a new method to simulate the behavior of a photovoltaic system. In particular, a practical method to determine the current voltage and the power voltage characteristics of a photovoltaic module, and then of photovoltaic strings and fields, has been demonstrated. The innovative feature is that the method does not require measurements of electrical module characteristics as only the electrical data provided in a customary photovoltaic module data sheet are used. This is a great advantage in order to simulate simply and quickly photovoltaic systems. The method has been applied to the experimental University of Trieste plant in order to determine its behavior during a year of operations.

Following the determination of the photovoltaic system behavior, a comparative economic analysis considering string and centralized solutions for a grid connected photovoltaic system has been proposed. The result of this comparison has been that, if particular shading effects are not present in the installation site, the centralized solution gives a shorter pay back period and therefore better economic productivity. Moreover, the economic analysis highlights there are a few misunderstandings in evaluating the Balance Of System since the photovoltaic field maximum power point is sometimes determinate erroneously.

By introducing an innovative photovoltaic field simulator, a solution to this problem has been proposed. The simulator will enable us to determine the power conditioning unit behavior with regard to its performance in following the field

maximum power point which changes with time in consequence of the particular climate conditions (of irradiance and temperature). It will also be used to investigate solar cell behavior under the same conditions. This will mean we have a more accurate value of the Balance Of System allowing a better analysis of the photovoltaic system behavior and thus a more effective economic analysis.

Other useful experimental aspects connected to the use of the simulator have been proposed. Useful tests will enable us to check the declared inverter efficiency, to determine its efficiency under specified conditions (i.e. the efficiency achieved when using the power conditioning unit at different latitudes), to check the inverter DC voltage range, etc.

Finally, the utility of the simulator in designing solar cell materials working in a real photovoltaic systems has been shown. Particular attention has been given to thin-film technologies because of the problems which these technologies may cause in MPPT operations in following the photovoltaic field maximum power point when shaded conditions along the photovoltaic field occur.

The review of photovoltaic field simulators, drawing on the conclusions of the proposed simulator might well be considered innovative because of its high nominal power (the power converter is rated 20kW), the possibility to connect with an inverter and finally, because of its control system which is implemented in a commercial CPU enabling us to change the simulation parameters (for example irradiance values investing the simulated photovoltaic field) in real time.

Moreover, the use of the photovoltaic field simulator will be useful in order to validate several issues discussed in sections three and four.

Appendix A

The University of Trieste plant

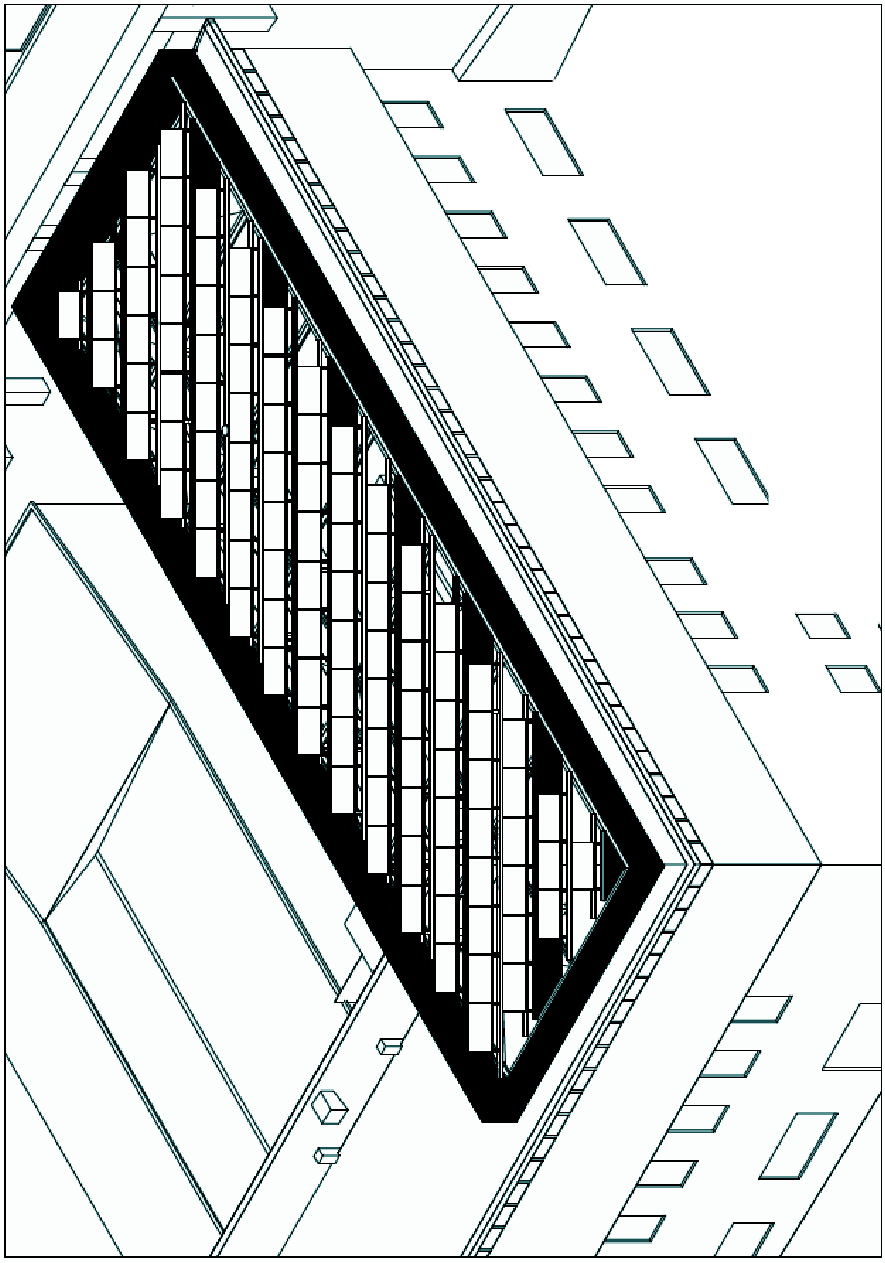

Figure A.1: The University of Trieste plant

Appendix B

Photovoltaic module data sheets

HIT PHOTOVOLTAIC MODULE
HIP-215NHE5

SANYO

The SANYO HIT (Heterojunction with Intrinsic Thin layer) solar cell is made of a thin mono crystalline silicon wafer surrounded by ultra-thin amorphous silicon layers. This product provides the industry's leading performance and value using state-of-the-art manufacturing techniques.

Benefit in Terms of Performance

High efficiency cell: 19.3%, Module: 17.2%
The HIT cell and module have the world's highest level of conversion efficiency in mass production.

High performance at high temperatures
Even at high temperatures, the HIT solar cell can maintain higher efficiency than a conventional crystalline silicon solar cell.

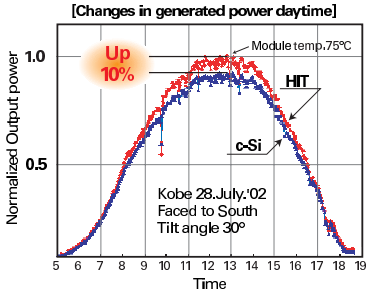

Environmental Friendly Solar Cell

More Clean Energy
HIT can generate more annual power output per unit area than other conventional crystalline silicon solar cells.

Special Features
SANYO HIT solar modules are 100% emission free, have no moving parts and produce no noise.
The dimensions of the HIT modules allow space-saving installation and achievement of maximum output power possible on given roof area.

Benefit in Terms of Quality

High quality in accordance with ISO 9001 and 14001 standards
HIT solar cell and modules are subject to strict inspections and measurements to ensure compliance with electrical, mechanical and visual criteria.

HIT Solar Cell Structure

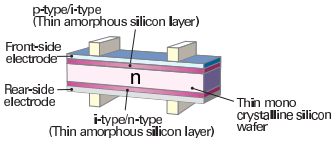

Development of HIT solar cell was supported in part by the New Energy and Industrial Technology Development Organization (NEDO).

Electrical and Mechanical Characteristics

HIP-215NHE5

Electrical data

Maximum power (Pmax)	[W]	215
Max. power voltage (Vpm)	[V]	42.0
Max. power current (Ipm)	[A]	5.13
Open circuit voltage (Voc)	[V]	51.6
Short circuit current (Isc)	[A]	5.61
Warranted minimum power (Pmin)	[W]	204.25
Output tolerance	[%]	+10/-5
Maximum system voltage	[Vdc]	1000
Temperature coefficient of Pmax	[%/°C]	- 0.30
Voc	[V/°C]	- 0.129
Isc	[mA/°C]	1.68

Note 1: Standard test conditions: Air mass 1.5, Irradiance = 1000W/m², Cell temperature = 25°C
Note 2: The values in the above table are nominal.

Dimensions and weight

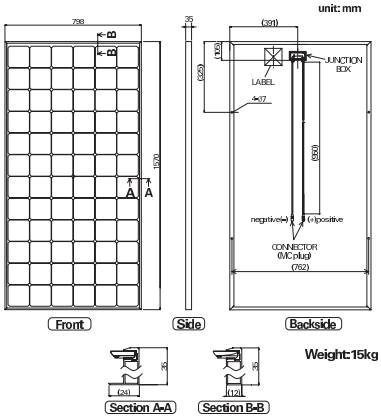

Dependence on irradiance

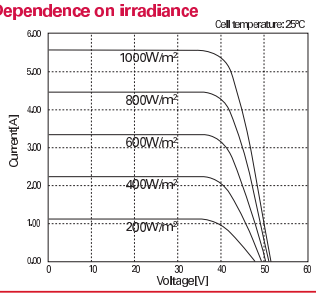

Dependence on temperature

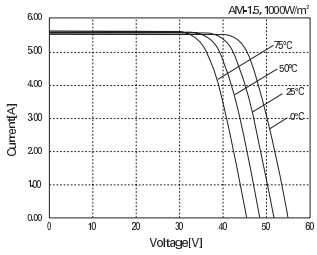

Certificates

IEC 61215

Electrical Protection Class II

Please consult your local dealer for more information.

www.solar-wind.co.uk

Warranty

Power output: 20 years (80% of minimum output power)
Product workmanship: 2 years
(Based on contract terms.)

⚠ **CAUTION!** Please read the operating instructions carefully before using the products.

Owing to our policy of continual improvement the products covered by this brochure may be changed without notice.

SANYO

SANYO Component Europe GmbH
Clean Energy Division

Stahlgruberring 4
81829 Munich, Germany
TEL: +49-(0)89-46 00 95-0
FAX: +49-(0)89-46 00 95-170
http://www.sanyo-component.com
email: info.solar@sanyo-component.com

SANYO Electric Co., Ltd.
Component Group, Clean Energy Company

5 - 5, Keihan-Hondori 2, Moriguchi,
Osaka 570-8677, Japan
TEL: +81-(0)6-69 94-7282
FAX: +81-(0)6-69 94-7289
http://www.sanyo.co.jp/clean/solar/hit_e/index_e.html
email: sola1011115@sanyo.co.jp

03/06

HIGH PERFORMANCE PHOTOVOLTAIC MODULES "SERIES "H"

MEASUREMENT CONDITIONS

(The electrical specifications are measured under irradiance level of 1000W/m2, 1,5 Air Mass Spectrum, cell temperature of 25°C)

SPECIFICATIONS

Cells	Monocrystalline 125mmx125mm pseudo square
Number of cells	72 series connected
Typical application	24V DC
Maximum voltage	600V DC
Size	mm 1596 (L) x 798 (W) x 40 (H)
Weight	17 Kg
Front glass	4 mm thick

TOLERANCE

Parameter	Values	Unit
Operating temperature	-40 + 85	°C
Hail diameter @ 80Km/h	Up to 25	mm
Continuous wind pressure	Up to 130	Km/h

CONNECTION TERMINALS

Connector type	1,90m wire (4,5mm² ø with MC connector)

ELETTRICAL TYPICAL VALUES (²)

Model	Max power **Pm**	Tolerance on **Pm** (¹)	Voltage @ Pm, **Vm**	Current @ Pm, **Im**	Open circuit voltage **Voc**	Short circuit current, **Isc**
SOL 155H	155W	+/- 2.5W	34.2V	4.5A	43.4V	5.2A
SOL 160H	160W	+/- 2.5W	34.8V	4.6A	43.5V	5.2A
SOL 165H	165W	+/- 2.5W	35.7V	4.6A	44.0V	5.2A
SOL 170H	170W	+/- 2.5W	36.1V	4.7A	44.2V	5.2A
SOL 175H	175W	+/- 2.5W	36.4V	4.8A	44.3V	5.2A
SOL 180H	180W	+/- 2.5W	37.2V	4.8A	44.4V	5.2A
NOCT: 48°C			Temperature coefficient Voltage: - 160.0 mV/°C Temperature coefficient Current: + 1.4 mA/°C Temperature coefficient Power: - 0.4 %/°C			

Note¹: defined as standard deviation of thousands measurements. Absolute power values depend on the measuring system. They can differ by +/- 3% from one measuring system to another.
Note²: Values averaged on thousands module measurements.

Characteristic curves

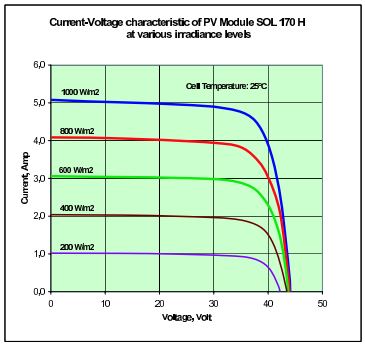

Size

Anodized Aluminium Frame

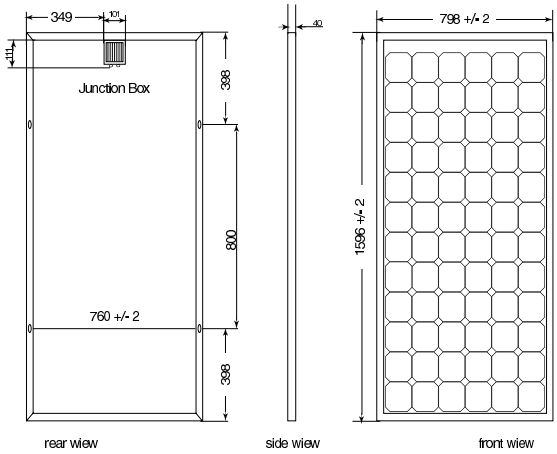

SOLTERRA FOTOVOLTAICO SA - VIA MILANO 7 - 6830 CHIASSO - SWITZERLAND
TEL. +41 91 6954060 - FAX +41 91 6954070 - WWW.SOLTERRA.CH - info@solterra.ch

HIGH PERFORMANCE PHOTOVOLTAIC MODULES "SERIES "H"

Solterra Fotovoltaico SA

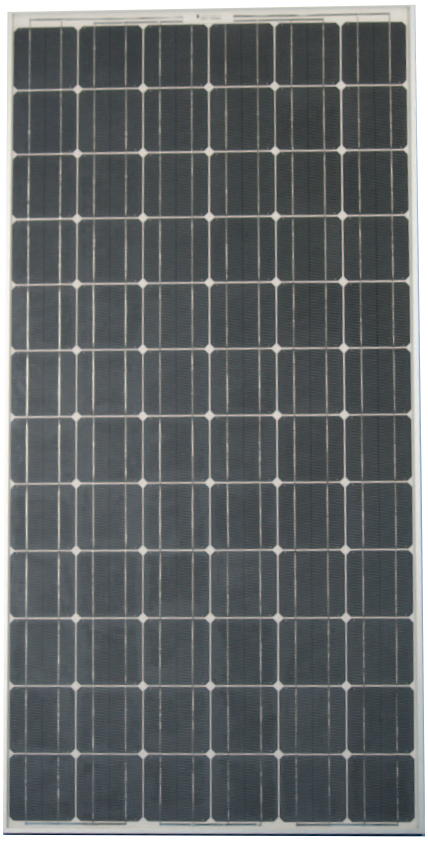

SOL 155H - SOL 160H
SOL 165H - SOL 170H
SOL 175H - SOL 180H

Monocrystalline
Photovoltaic Modules

MAIN FEATURES

1 **PV cells**: high power with 125mm x 125mm "pseudo-square" monocrystalline silicon.
2 **Front side**: textured tempered high transmittance glass.
3 **Encapsulant**: EVA pottant, UV stabilised.
4 **Back side**: PVF/PET/PVF.
5 **Junction Box**: IP 55 waterproof junction box equipped with 3-bypass diodes for an effective protection against hot spots.
Fast connectors for easy mounting.

CERTIFICATION

Modules qualified according to:
IEC 61215

WARRANTY

- 90% power output for 10 years
- 80% power output for 25 years

SOLTERRA FOTOVOLTAICO SA - VIA MILANO 7 - 6830 CHIASSO - SWITZERLAND
TEL. +41 91 6954060 - FAX +41 91 6954070 - WWW.SOLTERRA.CH - info@solterra.ch

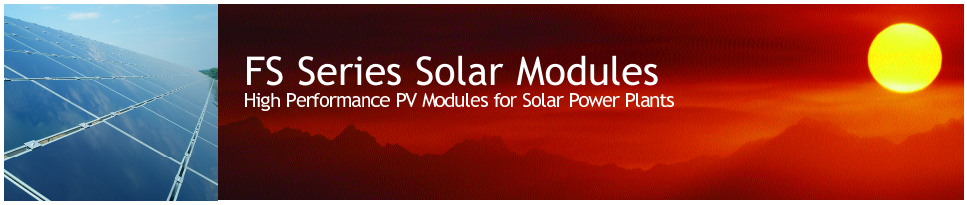

First Solar FS Series PV Modules

First Solar FS Series solar modules provide a product platform designed to reliably produce higher energy yield from solar power plants during the dynamic range of operating conditions.

Key Features

- Stable power output warranted for 20 years
- Very thin layers of compound semiconductor material provide cost effective energy production
- Low Temperature Coefficients provide greater energy production in real world operating conditions
- Optimized for applications where high output voltage is desirable
- UL1703 Listed for electrical and fire safety (class C fire rating)
- IEC61646 Certified
- Weatherproof connector and cordplate eliminate the need for a junction box and module-to-module field wiring
- Heat strengthened 3.2mm glass superstrate laminated to 3.2mm tempered back glass
- Designed for efficient recycling

First Solar

First Solar
4050 E. Cotton Center #6-68
Phoenix, AZ 85040

Tel: 602-414-9300
Fax: 602-414-9400
Email: info@firstsolar.com
Web: www.firstsolar.com

AZ-5-307 0404

FS Series Laminate Modules
Laminates can be easily integrated into different solar system designs and are compatible with many mounting clip systems used in ground mounted or building rooftop mounted solar power plants.

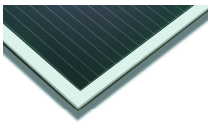

FS Series Laminate Module

FS-50
FS-55

FS-D Series Modules with Rails
Mounting Rails are attached to the FS Series modules to provide quick and easy mounting on racks or commercial structures.

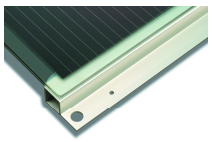

FS Series Module with Rail

FS-50 D
FS-55 D

Mechanical Specifications

	Laminate		With Rail	
	inches	cm	inches	cm
Length	47.25	120.00	47.25	120.00
Width	23.63	60.00	25.37	64.40
Thickness	0.25	0.60	1.20	3.00
	ft²	m²	ft²	m²
Area	7.75	0.72	7.75	0.72
	lbs	kg	lbs	kg
Weight	25	11.40	27	12.25

Electrical Specifications (+/- 10%)

Nominal Values		FS-50	FS-55
Nominal Power	P_{mpp}	50 W	55 W
Voltage at mpp	V_{mpp}	58 V	60 V
Current at mpp	I_{mpp}	0.87 A	0.92 A
Open Circuit Voltage	V_{oc}	85 V	88 V
Short Circuit Current	I_{sc}	1.08 A	1.09 A
Series Fuse Rating	AMPS	2A	
Normal Operating Cell Temp	NOCT	45 °C	
Maximum System Voltage	Volts	600 VDC	
Temperature Coefficient of P_{mpp}	$T_K(P_{mpp})$	-0.25%/°C	
Temperature Coefficient of V_{oc}	$T_k(V_{oc})$	-0.22%/°C	
Temperature Coefficient of I_{sc}	$T_k(I_{sc})$	+0.04%/°C	

* Electrical data is taken at Standard Test Conditions (STC): Irradiance of 1000W/m² with spectrum AM1.5 and a cell temperature of 25°C

Illuminated I-V Curve FS-50

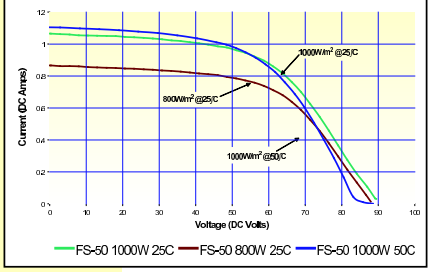

Illuminated I-V Curve FS-55

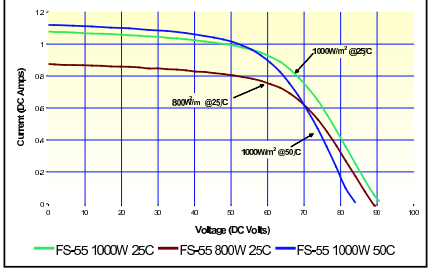

Mechanical Drawing (FS-D Series Module with Rail)

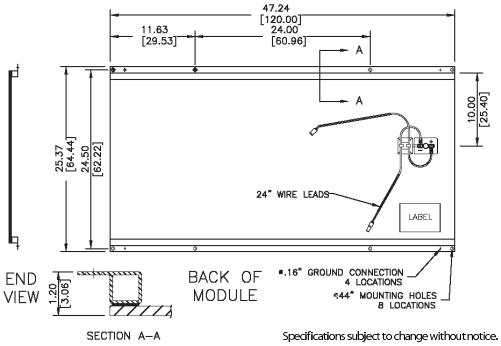

Specifications subject to change without notice.

IEC 61646 Certified

AZ-5-307 0404

First Solar®

Corporate & Marketing
4050 East Cotton Center 6-68
Phoenix, AZ 85040 USA

Tel: 602.414.9300
Fax: 602.414.9400
Email: info@firstsolar.com
www.firstsolar.com

First Solar GmbH
Wilhelm-Wolff-Str. 27
D-99099 Erfurt

Tel: +49 361 663399 60
Fax: +49 361 663399 65
Email: d-info@firstsolar.com
www.firstsolar.com/de